CD163+ macrophages promote angiogenesis and vascular permeability accompanied by inflammation in atherosclerosis

Liang Guo,[1] Hirokuni Akahori,[2] Emanuel Harari,[1] Samantha L. Smith,[1] Rohini Polavarapu,[2] Vinit Karmali,[2] Fumiyuki Otsuka,[1] Rachel L. Gannon,[1] Ryan E. Braumann,[1] Megan H. Dickinson,[1] Anuj Gupta,[3] Audrey L. Jenkins,[4] Michael J. Lipinski,[4] Johoon Kim,[5] Peter Chhour,[5] Paul S. de Vries,[6] Hiroyuki Jinnouchi,[1] Robert Kutys,[1] Hiroyoshi Mori,[1] Matthew D. Kutyna,[1] Sho Torii,[1] Atsushi Sakamoto,[1] Cheol Ung Choi,[2] Qi Cheng,[1] Megan L. Grove,[6] Mariem A. Sawan,[3] Yin Zhang,[7] Yihai Cao,[7] Frank D. Kolodgie,[1] David P. Cormode,[5] Dan E. Arking,[8] Eric Boerwinkle,[6,9] Alanna C. Morrison,[6] Jeanette Erdmann,[10] Nona Sotoodehnia,[11] Renu Virmani,[1] and Aloke V. Finn[1,3]

[1]CVPath Institute, Gaithersburg, Maryland, USA. [2]Department of Medicine, Emory University School of Medicine, Atlanta, Georgia, USA. [3]Department of Medicine, University of Maryland School of Medicine, Baltimore, Maryland, USA. [4]MedStar Heart and Vascular Institute and MedStar Health Research Institute, MedStar Washington Hospital Center, Washington, DC, USA. [5]Department of Radiology, Perelman School of Medicine, University of Pennsylvania, Philadelphia, Pennsylvania, USA. [6]Human Genetics Center, Department of Epidemiology, Human Genetics, and Environmental Sciences, School of Public Health, The University of Texas Health Science Center at Houston, Houston, Texas, USA. [7]Department of Microbiology, Tumor and Cell Biology, Karolinska Institute, Stockholm, Sweden. [8]McKusick-Nathans Institute of Genetic Medicine, Johns Hopkins University School of Medicine, Baltimore, Maryland, USA. [9]Human Genome Sequencing Center, Baylor College of Medicine, Houston, Texas, USA. [10]Institute for Cardiogenetics, University of Lübeck, and German Centre for Cardiovascular Research (DZHK), Partner Site Hamburg/Kiel/Lübeck, Germany. [11]Division of Cardiology, Department of Medicine and Epidemiology, Cardiovascular Health Research Unit, University of Washington, Seattle, Washington, USA.

Intake of hemoglobin by the hemoglobin-haptoglobin receptor CD163 leads to a distinct alternative non–foam cell antiinflammatory macrophage phenotype that was previously considered atheroprotective. Here, we reveal an unexpected but important pathogenic role for these macrophages in atherosclerosis. Using human atherosclerotic samples, cultured cells, and a mouse model of advanced atherosclerosis, we investigated the role of intraplaque hemorrhage on macrophage function with respect to angiogenesis, vascular permeability, inflammation, and plaque progression. In human atherosclerotic lesions, CD163+ macrophages were associated with plaque progression, microvascularity, and a high level of HIF1α and VEGF-A expression. We observed irregular vascular endothelial cadherin in intraplaque microvessels surrounded by CD163+ macrophages. Within these cells, activation of HIF1α via inhibition of prolyl hydroxylases promoted VEGF-mediated increases in intraplaque angiogenesis, vascular permeability, and inflammatory cell recruitment. CD163+ macrophages increased intraplaque endothelial VCAM expression and plaque inflammation. Subjects with homozygous minor alleles of the SNP rs7136716 had elevated microvessel density, increased expression of CD163 in ruptured coronary plaques, and a higher risk of myocardial infarction and coronary heart disease in population cohorts. Thus, our findings highlight a nonlipid-driven mechanism by which alternative macrophages promote plaque angiogenesis, leakiness, inflammation, and progression via the CD163/HIF1α/VEGF-A pathway.

Introduction

Macrophages play a critical role in atherogenesis but are a heterogeneous group of immune cells (1). The atherosclerotic plaque microenvironment is an important stimulus driving their differentiation into distinct cell types that undoubtedly influence plaque evolution. Our understanding of how these stimuli affect macrophage behavior and in turn influence atherosclerosis remains incomplete (2).

▶ Related Commentary: p.910

Authorship note: L. Guo, H. Akahori, and E. Harari contributed equally to this work.
Conflict of interest: The authors have declared that no conflict of interest exists.
Submitted: February 13, 2017; **Accepted:** January 2, 2018.
Reference information: *J Clin Invest*. 2018;128(3):1106–1124.
https://doi.org/10.1172/JCI93025.

Prevailing paradigms describe atherosclerosis as a Th1-driven disease, focusing on the role of lipids as a primary stimulus driving proinflammatory M1 macrophage responses (3). Within this context, monocytes are initially recruited to the subendothelial space by entrapped oxidized low-density lipoprotein. In the intimal space, macrophages scavenge lipoproteins to become foam cells, which secrete proinflammatory molecules and other factors leading to plaque progression.

Alternatively polarized macrophages (sometimes referred to as M2) are thought to counterbalance M1 responses by promoting the resolution of inflammation and promoting tissue repair (4). Although M2 macrophages have recently been described within human atherosclerotic specimens, their role in influencing plaque structure and evolution remains uncertain (5). One important stimulus for alternative macrophage conversion within human atherosclerosis is intraplaque hemorrhage (IPH),

which is thought to result from plaque neovascularization and increased microvessel permeability (6, 7). These features are considered critical elements of advanced atherosclerotic plaques and are linked to plaque progression through the accumulation of erythrocyte membranes, which are rich in free cholesterol and promote necrotic core enlargement (8).

Within areas of IPH, oxidative stress leads to erythrocyte lysis, which releases free hemoglobin (Hb) (9). Hb is quickly bound by the plasma protein haptoglobin, and hemoglobin:haptoglobin (HH) complexes are internalized into the macrophage via the CD163 receptor exclusively expressed on cells of this lineage (10, 11). We and others have previously shown that intake of HH by CD163 leads to a distinct phenotype of macrophage termed M(Hb) (also referred to as Mhem) found in areas of neoangiogenesis and hemorrhage characterized by high surface expression of CD163, reduced proinflammatory cytokine production, and a lack of lipid retention, all characteristics which distinguish them from foamy macrophages (6, 12). On the basis of these findings, the M(Hb) macrophage has been termed atheroprotective (12, 13). However, the association of M(Hb) macrophages with areas of intraplaque angiogenesis and permeability raises the important question of whether these cells are merely bystanders or play an active role in these processes.

An abundance of extracellular ferric iron and lowered ROS formation are important features defining areas in which M(Hb) macrophages are found (6). We have previously shown that increased export of iron through upregulation of the iron exporter ferroportin (FPN) lowers intracellular free iron within M(Hb) macrophages (6, 14). A relationship between iron and the proangiogenic transcription factor HIF1α can be found through its interactions with the prolyl hydroxylase proteins (PHDs). Under conditions of normoxia or hyperoxia, HIF1α becomes hydroxylated by PHDs on proline residues 402 and 564, within its oxygen-dependent domain. This allows it to be recognized by the von Hippel–Lindau tumor-suppressor protein (pVHL), which targets it for ubiquitin-mediated degradation (15). While hypoxia is a well-known activator of HIF1α, iron itself also indirectly controls the activation of HIF1α by serving as an essential cofactor for the activity of PHDs (16). Although 3 HIF prolyl hydroxylases (PHD1, PHD2, PHD3) mediate the hydroxylation of proline residues on HIF1α, PHD2 is responsible for more than 95% of the activity in cultured cells (17). PHD2 hydroxylase activity is stimulated by the addition of iron in vitro, and its activity is inhibited by iron chelators (16). Thus, changes in iron metabolism within M(Hb) macrophages might affect their angiogenic potential via inhibition of PHDs.

Here, we reveal an important molecular pathway within alternatively polarized M(Hb) macrophages that promotes intraplaque angiogenesis, permeability, inflammatory cell recruitment, and plaque progression in human atherosclerosis. Intracellular iron deprivation within M(Hb) macrophages inhibits PHD2 activity, which leads to the accumulation of HIF1α and VEGF-A. Using human atherosclerotic specimens and in vitro assays with human cells, we demonstrate that M(Hb) macrophages are associated with intraplaque angiogenesis, defective endothelial junctional protein expression, and increased vascular inflammation mediated through VEGF-A–VEGFR2 interactions. Genetic deletion of CD163 in a mouse model of IPH reduced plaque permeability, progression, and inflammatory cell recruitment. These findings demonstrate an unexpected but important proatherogenic role for M(Hb) macrophages in the response to IPH by promoting plaque angiogenesis and permeability. Moreover, these studies point toward the HIF1α/VEGF-A system as a potential target for antiatherosclerotic therapies.

Results

Human carotid plaque pathological characterization, plaque progression, and association with CD163⁺ macrophages. A total of 60 atherosclerotic samples from patients undergoing surgical carotid endarterectomy (CEA) were available in the CVPath Registry (18). A detailed history was not included for 22 of these samples, and they were therefore excluded. Thirty-eight specimens containing culprit segments along with proximal and distal (flanking) segments were available for analysis and assessed for plaque morphology. We classified 114 plaques (38 culprit, 38 proximal flanking, and 38 distal flanking plaques) and performed IHC to assess each one for the area occupied by CD163, a marker of M(Hb) macrophages. We found a strong positive correlation between CD163⁺ macrophage area and plaque progression (i.e., pathological intimal thickening [PIT] or intimal xanthoma, fibroatheroma or thin-cap fibroatheroma (TCFA), and plaque rupture or healed rupture) (Figure 1, A and B). The correlation with plaque progression could also be demonstrated by stratifications of stenosis and necrotic area percentage (Figure 1, C and D). These results suggest a strong association between CD163 expression in alternative macrophages and atherosclerotic disease progression.

Human carotid plaque assessment of angiogenesis in high and low CD163/CD68 plaque areas. We also used IHC to assess each plaque for the area occupied by the general macrophage marker CD68. Areas were separated into low and high CD163 expression on the basis of their CD163/CD68 ratio (low CD163/CD68 <0.20 vs. high CD163/CD68 >0.70). (Foam cells predominated in the low CD163 areas.) We determined the extent of microvascularity in each of these areas using antibodies against CD31 and vWF. Table 1 shows that the total content of macrophages in each area (as assessed by CD68 expression) was not significantly different between groups. The microvessel number per unit area, however, was significantly greater within high CD163 areas (Table 1, see also representative images in Figure 1, E and F). Because most microvessels were seen around CD16⁺ M(Hb) cells both within low and high CD163 plaque areas, we further subdivided each area into CD163⁻ and CD163⁺ regions for a local effect assessment in the plaque. Regardless of a high or low CD163/CD68 ratio, we detected greater numbers of microvessels in regions that had CD163⁺ macrophages (CD163⁺ area in Table 1). This suggests that CD163⁺ macrophages are associated with plaque angiogenesis.

Alternative CD163⁺ macrophages express HIF1α and VEGF-A and are associated with intraplaque angiogenesis and vascular permeability. We next evaluated the expression of the proangiogenic transcription factor HIF1α and its transcriptional target VEGF-A using similar methodology. High CD163 areas demonstrated heavy expression of HIF1α and VEGF-A compared with CD163 low/foam cell–rich areas (Figure 2A). HIF1α was predominantly located within CD163⁺ macrophages. To confirm our findings, protein was extracted from high CD163 plaques and compared with protein

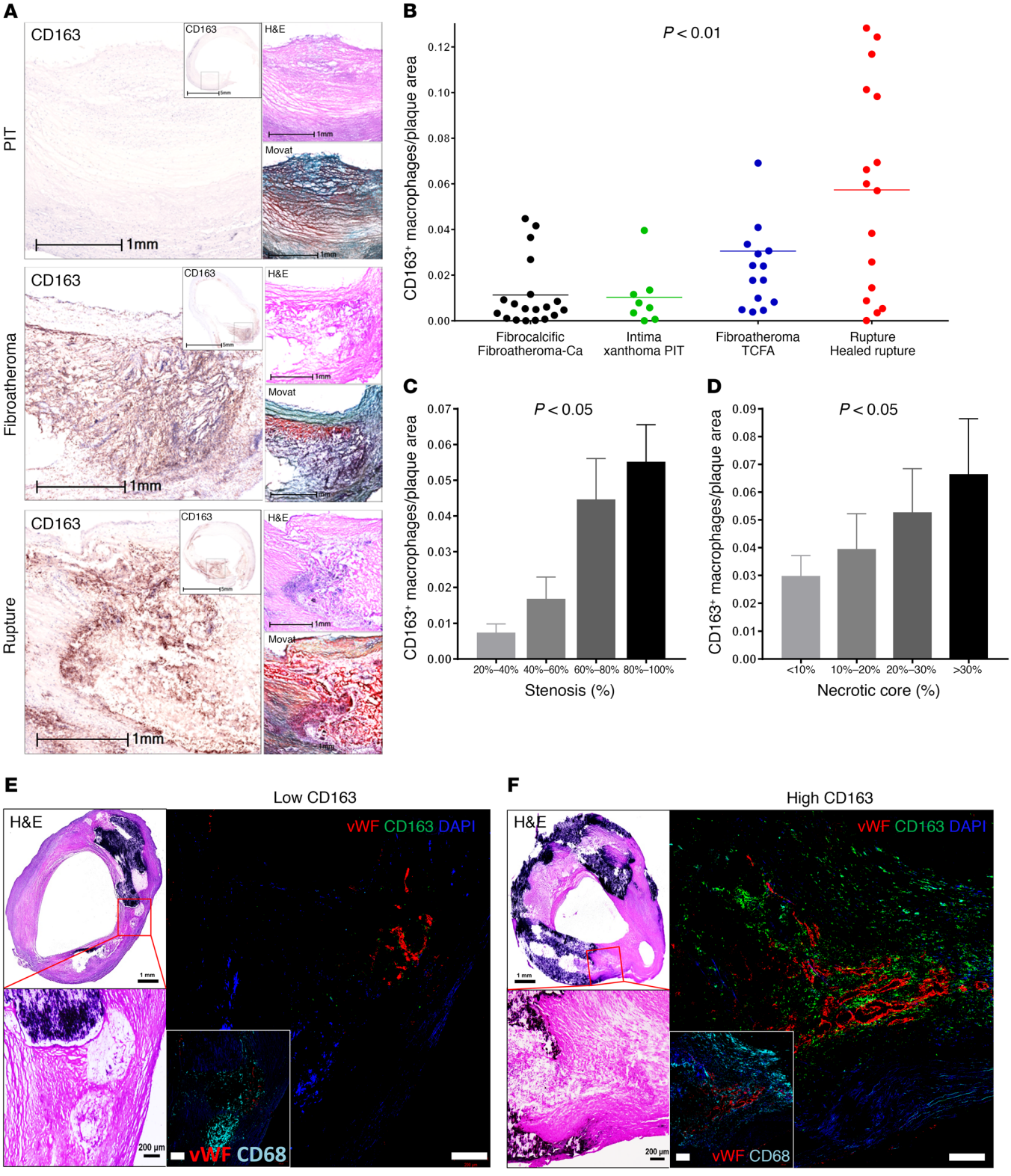
A
PIT
Fibroatheroma
Rupture
CD163
H&E
Movat
1mm
B
P < 0.01
CD163+ macrophages/plaque area
0.00
0.02
0.04
0.06
0.08
0.10
0.12
Fibrocalcific Fibroatheroma-Ca
Intima xanthoma PIT
Fibroatheroma TCFA
Rupture Healed rupture
C
P < 0.05
CD163+ macrophages/plaque area
0.00
0.01
0.02
0.03
0.04
0.05
0.06
0.07
20%–40%
40%–60%
60%–80%
80%–100%
Stenosis (%)
D
P < 0.05
CD163+ macrophages/plaque area
0.00
0.01
0.02
0.03
0.04
0.05
0.06
0.07
0.08
0.09
<10%
10%–20%
20%–30%
>30%
Necrotic core (%)
E
Low CD163
H&E
vWF CD163 DAPI
vWF CD68
200 μm
F
High CD163
H&E
vWF CD163 DAPI
vWF CD68
200 μm

Figure 1. CD163$^+$ macrophages are associated with progression of carotid atherosclerosis in humans. (**A**) Representative images of human carotid arteries with PIT, fibroatheromatous, and ruptured atherosclerotic plaques. High-magnification IHC images of CD163 with low-magnification insets. H&E and Movat pentachrome stains are also shown. Scale bars: 1 mm and 5 mm (insets). (**B**–**D**) Correlation between CD163$^+$ macrophages and human carotid plaque progression. (**B**) Human carotid plaques were classified as fibrocalcific or fibroatheroma with calcification (Fibroatheroma-Ca) (n = 19, black); intima xanthoma or PIT (n = 8, green); fibroatheroma or TCFA (n = 14, blue); and ruptured or healed rupture (n = 16, red), with the corresponding percentage of CD163$^+$ macrophages per plaque area. (**C**) Correlation between CD163$^+$ macrophages and the percentage of stenosis. The percentage of stenosis was categorized as follows: 20%–40% (n = 5); 40%–60% (n = 14); 60%–80% (n = 23); and 80%–100% (n = 28). (**D**) Correlation between CD163$^+$ macrophages and the percentage of necrotic core area. The percentage of necrotic core area was classified as: <10% (n = 32); 10%–20% (n = 19); 20%–30% (n = 9); and >30% (n = 10). (**E** and **F**) Human plaques from CEAs were examined by histology and immunofluorescence. Images were acquired by confocal microscopy using a ×20 objective (9 tiles, **E** and **F**), with optical slicing in the z axis. In **E**, as explained in the text, areas from fibroatheromatous lesions containing foam cell (CD163$^-$ [green], CD68$^+$ [cyan]) macrophages (i.e., low CD163) and M(Hb) macrophages (CD163$^+$, CD68$^+$ [i.e., high CD163]) were immunostained using antibodies against vWF antigen for detection of microvessels. Nuclei were counterstained using DAPI (blue). Note that calcification is seen as dense areas of dark purple. Adjacent low- and high-magnification images of H&E-stained sections show the corresponding regions of angiogenesis. Scale bars: 1 mm and 200 μm. Results are presented as the mean or the mean ± SEM. For multiple group comparisons, 1-way ANOVA was used. P values shown in **B**–**D** were determined by 1-way ANOVA.

extracted from low CD163 plaques, and immunoblotting was performed for both HIF1α and VEGF-A (CD68 staining intensity was not different between the 2 areas). Western blotting confirmed that plaques rich in CD163$^+$ M(Hb) cells had greater HIF1α and VEGF-A expression than did low CD163 plaques (Figure 2B). To visualize CD163 and VEGF transcript levels at a single-cell level concurrently in CD163$^+$ macrophages, we performed RNAscope analysis, a new ISH technique for the detection of RNA within intact cells, using CD163 and VEGF dual probes. This high-resolution, single RNA molecule signal of CD163 and VEGF transcripts showed high VEGF expression in macrophages expressing high CD163 transcripts (≥5 CD163 dots per cell) compared with those with low CD163 transcripts (1–4 CD163 dots per cell) (Figure 2, C and D).

M(Hb) and microvascular permeability within intraplaque vessels. Our previous findings as well as those by others suggest that microvessels located within advanced atherosclerotic plaques show compromised endothelial morphology and integrity, characterized by loss of VE-cadherin, the major protein responsible for the maintenance of endothelial barrier function (19, 20). To explore the relationship between M(Hb) cells and defects in endothelial permeability, we stained sections of advanced atherosclerotic plaques for VE-cadherin and vWF, which is released upon endothelial damage and stains diffusely in leaky endothelium (21). In comparison with microvessels in close proximity to areas rich in foam cell macrophages (low CD163), microvessels near CD163$^+$ macrophages (high CD163) had significantly less continuous formation of VE-cadherin coverage, while showing diffuse perivascular staining for vWF (Figure 2, E and F). These results suggest that CD163$^+$ M(Hb) cells are associated with areas of intraplaque angiogenesis containing defective endothelial barrier function.

Inhibition of PHDs by relative iron deprivation within M(Hb) cells increases HIF1α/VEGF-A and promotes angiogenesis. We previously demonstrated that human plaque areas rich in M(Hb) cells had reduced ROS, signs of oxidative damage, and an abundance of ferric iron, consistent with iron release from macrophages (6). CD163$^+$ M(Hb) cells can be reproduced in vitro by differentiation of human monocytes over 5 to 7 days in HH-enriched media (6). Hb/iron intake into macrophages causes an increase in the iron-binding protein ferritin and upregulation of the iron exporter FPN, which results in significant lowering of intracellular free iron (6, 22). By laser capture microdissection, lesion areas with high levels of CD163$^+$ macrophages (high CD163) in human carotid plaques showed elevated FPN expression compared with areas containing low levels of CD163$^+$ macrophages (low CD163) (Figure 2G). Consistent with this, HH-differentiated macrophages had lower levels of intracellular free iron (Figure 3A). Because PHD2 function is dependent on iron as a cofactor, we examined PHD2 activity using cellular lysates from human macrophages differentiated in HH-enriched media. Lysates were exposed to a peptide derived from the HIF1α oxygen–dependent degradation domain, and hydroxylation was measured using an antibody specific for hydroxylated HIF1α (Pro564). We found that PHD2 activity was significantly lower in HH-differentiated cells (Figure 3B). To confirm our results, we measured hydroxylated HIF1α (HIF1α-OH) levels in control and HH-differentiated macrophages in the presence of 10 μM MG132, a proteasome inhibitor, using an antibody against HIF1α-OH. We found that HIF1α-OH levels were significantly lower in HH-differentiated cells (Figure 3C). There were no changes in the total amount of PHD2 levels by Western blotting in control or HH-differentiated cells (Figure 3D). Next, to confirm relative iron deprivation as the cause of elevated HIF1α levels, we used 2 different approaches. First, we modulated intracellular iron by treating HH-differentiated cells with hepcidin, a peptide whose major function is to degrade FPN (23). Hepcidin given 24 hours before harvesting was able to increase intracellular iron within HH-differentiated macrophages but had no effect on control cells (Supplemental Figure 1A; supplemental material available online with this article; https://doi.org/10.1172/JCI93025DS1). HIF1α levels were significantly increased in HH-differentiated cells and dramatically decreased to control levels after hepcidin treatment, while there was no effect on control-treated cells (Figure 3E). We observed similar results for VEGF-A levels, which were determined by ELISA analysis of supernatants of these cells (Figure 3F). HIF1α levels were also decreased in HH-differentiated cells when iron (10, 50, or 100 μM $FeCl_3$) was added directly to them 24 hours before harvesting (Supplemental Figure 1B). Last, to confirm the angiogenic ability of M(Hb) cells, supernatants from control and HH-treated macrophages, with or without added hepcidin, were evaluated in an in vitro Matrigel angiogenesis assay using human aortic endothelial cells (HAECs). Tube formation was increased by more than 2-fold with HH supernatants, but was not significantly changed in the presence of hepcidin (Figure 3G). These data suggest that relative iron deprivation within M(Hb) cells inhibits PHD2 activity to increase HIF1α-mediated angiogenesis.

CD163$^+$ M(Hb) cells promote vascular permeability via VEGF-A/VEGFR2 signaling. HIF1α accumulation within M(Hb) cells drives the transcription of VEGF-A, a key regulator of endothelial per-

Table 1. Macrophage content and angiogenesis in human carotid plaques

	Low CD163		High CD163		*P* value
Macrophages					
CD163/CD68 (ratio)	0.09 ± 0.07		0.90 ± 0.13		< 0.01
Total CD163 area (mm^2)	0.10 ± 0.09		1.39 ± 0.88		< 0.01
% Area positive for CD163	0.30 ± 0.23		3.10 ± 1.65		< 0.01
Total CD68 area (mm^2)	1.10 ± 0.61		1.54 ± 0.90		NS
% Area positive for CD68	3.28 ± 1.64		3.40 ± 1.61		NS
Angiogenesis					
Microvessels/plaque area (n/mm^2)	0.72 ± 0.37		1.36 ± 0.87		< 0.05
Microvessels (n)	$CD163^+$ [A]19.00 ± 8.68	$CD163^-$ 3.50 ± 2.64	$CD163^+$ [A]48.20 ± 23.02	$CD163^-$ 3.90 ± 3.67	< 0.01[A]

Results are presented as the mean ± SD (n = 10 plaques per group). All P values were determined by 2-sided Student's t test. [A]$P < 0.01$.

meability (24). Previous studies suggest that VEGFR2 activation by its major ligand VEGF-A leads to the formation of a complex among VEGFR2, VE-cadherin, and Src at intercellular junctions, and promotes specific tyrosine phosphorylation of VE-cadherin (24). This results in rapid internalization and degradation of VE-cadherin. To determine whether M(Hb) cells promote vascular permeability, we examined the effect of supernatants from human control or HH-differentiated macrophages on the permeability of HAECs using transendothelial electrical resistance (TEER) and FITC-dextran Transwell permeability assays. The supernatants of HH-differentiated macrophages caused a significant decrease in TEER and an increase in FITC-dextran permeability (both indicating greater permeability) compared with HAECs transfected with scrambled siRNA (Figure 4, A and B). However, knocking down VEGFR2 in endothelial cells by transfection of VEGFR2 siRNA completely abolished the increase in endothelial cell permeability after exposure to HH-differentiated macrophage supernatants in both assays (Figure 4, A and B). With respect to permeability, the behavior of endothelial cells treated with control supernatants did not change in the presence of VEGFR2 siRNA. We next examined the expression of VE-cadherin in cultured human endothelial cells transfected with scrambled or VEGFR2 siRNAs and exposed to HH-differentiated macrophage supernatants. There was distinct and characteristic staining for VE-cadherin in the plasma membrane of control-treated endothelial cells, which contrasted with the cells treated with M(Hb) supernatants that showed significantly less membrane staining but more internalization of VE-cadherin (Figure 4, C and D). Interestingly, endothelial cells transfected with VEGFR2 siRNA and treated with M(Hb) supernatants showed partial restoration of VE-cadherin in the plasma membrane (Figure 4, C and D). We confirmed this result by immunoblotting for VE-cadherin in membrane protein extractions (Figure 4, E and F). Collectively, these results suggest that M(Hb) macrophages promote endothelial permeability via VEGF-A/VEGFR2 signaling.

Deletion of CD163 in mice reduces intraplaque neovascularization and plaque progression. To explore the role of Hb in phenotypic modulation of macrophage behavior with respect to angiogenesis, we isolated peritoneal macrophages from CD163-knockout mice we had previously generated (25). Our published data as well as those of others suggest that mice can support a M(Hb) phenotype similar to that of humans (14, 26, 27). Exposure of peritoneal macrophages to mouse Hb (0.1 mg/ml) overnight resulted in significant upregulation of HIF1α by Western blotting and release of VEGF-A (Figure 5, A and B) in WT but not *CD163*$^{-/-}$ mice. (Ingestion of Hb by mouse $CD163^+$ macrophages does not seem to be as dependent on haptoglobin binding as human CD163 is [ref. 27].) Moreover, treatment of mouse dermal endothelial cells (MDECs) with supernatants from WT mouse peritoneal macrophages exposed to Hb resulted in significant increases in tube formation in an in vitro Matrigel angiogenesis assay (Supplemental Figure 2), a decrease in membrane VE-cadherin expression (Supplemental Figure 3), and an increase in membrane permeability (Supplemental Figure 4). There was no effect of supernatants from Hb-exposed, CD163-deficient macrophages in any of these assays with respect to these endpoints (Supplemental Figures 2–4). Collectively, these results suggest that CD163 mediates the proangiogenic and pro-permeability effects of Hb on macrophages.

To determine whether Hb is an important modulator of macrophage-mediated angiogenesis and permeability in the setting of atherosclerosis, we crossed *CD163*$^{-/-}$ mice with atherosclerosis-prone apolipoprotein E–deficient (*ApoE*$^{-/-}$) mice (both on a C57BL6 background). Because IPH is not typically observed in the aortic sinus after high-fat diet feeding in *ApoE* $^{-/-}$ mice, we examined the brachiocephalic arteries (BCAs) of aged, chow-fed mice, which reproducibly develop IPH (28). While we detected no differences in the aortic root plaque lesion areas in *ApoE*$^{-/-}$ *CD163*$^{-/-}$ versus *Apo E*$^{-/-}$ mice (Supplemental Figure 5), in 1-year-old *ApoE*$^{-/-}$ *CD163*$^{-/-}$ double-knockout mice, we observed a significant reduction in BCA plaque lesion area and intraplaque neovascularization and hemorrhage (by immunostaining using antibodies against VE-cadherin and Ter-119, respectively) (Figure 5, C–E, H, and I, and Supplemental Figure 9). One-year-old *ApoE*$^{-/-}$ and *ApoE*$^{-/-}$ *CD163*$^{-/-}$ mice had similar body weights, plasma cholesterol, glucose, and insulin levels (Supplemental Figure 6), and total numbers and types of WBCs (Supplemental Figure 7), as well as similarities in various measures of iron status (Supplemental Figure 8). $CD163^+$ macrophages were routinely seen in areas of angiogenesis within BCA plaques from *ApoE*$^{-/-}$ mice (Figure 5H). In comparison with *ApoE*$^{-/-}$ mice, *CD163*$^{-/-}$ *ApoE*$^{-/-}$ mice had significantly less BCA plaque complexity (Figure 5F), smaller necrotic areas (Figure 5G), and greater fibrous cap thickness (Supplemental Figure 10). To measure intraplaque neovascular permeability, FITC-dextran was administrated i.v. We found that intraplaque FITC-dextran, quantified by confocal microscopy, was reduced by more than 50% in *ApoE*$^{-/-}$ *CD163*$^{-/-}$ mice versus *ApoE*$^{-/-}$ controls, consistent with the lower microvessel density observed in *ApoE*$^{-/-}$ *CD163*$^{-/-}$ mice (Figure 5, I and J). These results collectively indicate that Hb and CD163 in particular are critical mediators of macrophage-mediated angiogenesis, vascular permeability, and plaque progression.

Microvascular endothelial cells surrounding CD163⁺ macrophages have elevated VCAM expression. VCAM has been shown to be critical in the development of atherosclerosis in experimental models, because it promotes inflammatory cell entry into the vessel wall (29). Intraplaque neovessels have been previously shown to express VCAM, which was associated with increased macrophage density (30). We hypothesized that CD163⁺ macrophages might also promote leukocyte entry into the plaque via VEGF-mediated increases in VCAM expression on intraplaque microvessels. HAECs treated with supernatant collected from macrophages differentiated with HH had significant increases in VCAM expression as detected by Western blotting (Figure 6, A and B). Immunofluorescence showed an increase in VCAM localization to the endothelial cells (using VE-cadherin antibody) in BCA plaques from *ApoE*$^{-/-}$ mice, whereas we observed little upregulation or colocalization in *ApoE*$^{-/-}$ *CD163*$^{-/-}$ mice (Figure 6, D and E). Similarly, we detected fewer macrophages in BCA plaques from *ApoE*$^{-/-}$ *CD163*$^{-/-}$ mice compared with *Apo E*$^{-/-}$ mice (Figure 6F).

The underlying mechanism of endothelial VCAM upregulation by CD163⁺ macrophages appeared to be related to the NF-κB signaling pathway, as Western blotting of HAECs treated with supernatant collected from macrophages differentiated with HH showed a greater phosphorylated NF-κB (p–NF-κB) (p65) to total NF-κB ratio (Figure 6, A and C) compared with those treated with supernatant from control macrophages. When cells were pretreated with the NF-κB inhibitor BAY 11-7082, VCAM upregulation by CD163⁺ M(Hb) macrophage supernatants was blocked (Supplemental Figure 11). Since VEGF is known to be able to upregulate VCAM in endothelial cells via activation of NF-κB (31), we examined whether VEGFR2 knockdown in the endothelial cells treated with control supernatants versus CD163⁺ M(Hb) macrophage supernatants could attenuate this inflammatory response. Indeed, knockdown of VEGFR2 by siRNA in cultured human endothelial cells blocked the upregulation of VCAM and NF-κB in endothelial cells treated with M(Hb) supernatants (Figure 6, G–I). Moreover, treatment of MDECs with supernatants from WT mouse peritoneal macrophages exposed to Hb resulted in a significant increase in VCAM expression; however, there was no effect of supernatants from Hb-exposed, CD163-deficient (*CD163*$^{-/-}$) macrophages (Supplemental Figure 12).

To confirm that VEGF mediated the increase in intraplaque endothelial VCAM expression and monocyte recruitment to the plaque, we performed studies in mice using a VEGF-blocking antibody and immunohistochemical analyses for VE-cadherin and VCAM colocalization and monocyte tracing. Six- to eight-month-old *ApoE*$^{-/-}$ mice were given a VEGF-blocking antibody or a control antibody via i.p. administration for 4 weeks. At the end of the antibody treatment, we injected gold-nanoparticle–labeled (Au-nanoparticle–labeled) monocytes i.v., measured monocyte infiltration into BCA plaques in serial histological sections, and performed immunohistochemical analyses using antibodies against VE-cadherin and VCAM. The results showed less VE-cadherin and VCAM colocalization in plaques from *ApoE*$^{-/-}$ mice treated with a VEGF-blocking antibody than was seen in plaques treated with the control antibody (Supplemental Figure 13) and a decrease in the number of labeled monocytes in BCA plaques after VEGF-blocking antibody treatment (Figure 6J). A third group of *ApoE*$^{-/-}$ *CD163*$^{-/-}$ mice were also treated with a control antibody, and few or no labeled monocytes could be found in the BCA plaques (Figure 6J).

We next evaluated the severity and distribution of inflammation in the human plaques by histological scoring. Macrophage areas with high CD63 expression were associated with significantly higher inflammation scores (Figure 6, K and L). Confocal immunofluorescence showed that the microvessels surrounding high CD163⁺ macrophages were associated with more CD3⁺ T cells (Figure 6, M and N). These mouse and human data suggest a critical role for CD163⁺ macrophages in promoting microvascular inflammation and leukocyte recruitment.

CD163⁺ macrophages are associated with increased angiogenesis, microvessel permeability, and intraplaque endothelial inflammation in human coronary artery plaques. To further explore the proangiogenic and pro-permeability roles of CD163⁺ macrophages in human coronary atherosclerotic disease, Evans blue dye (EBD) (complexed with albumin) staining, a commonly used method to determine microvascular permeability, was used to perfuse intact and freshly collected human coronary artery samples with evidence of advanced atherosclerosis. Cross-sectional examination of EBD-perfused coronary arteries revealed distinct areas of tissue staining within plaques (Figure 7A). Heavily EBD-stained areas were colocalized with intraplaque microvessels surrounded by CD163⁺ macrophages, as identified by immunofluorescence and confocal imaging (Figure 7A, positive area 1). VCAM was also shown to be colocalized with microvascular endothelial cells by VE-cadherin staining (Figure 7A, positive area 2). Quantitation of microvessels, CD163⁺ macrophages, and VCAM in EBD-positive versus EBD-negative areas showed significantly higher microvessel density, more CD163⁺ macrophages, and upregulated VCAM expression in EBD-positive versus EBD-negative areas in the plaque (Figure 7, B–D). These results suggest that areas of high microvascular permeability in human coronary artery lesions are associated with the presence of CD163⁺ macrophages and increased expression of endothelial VCAM.

Last, SNPs in the *CD163* gene were examined in a cohort of 346 African American patients from the CVPath Registry. Among the SNPs examined, homozygous G-allele carriers of rs7136716, an upstream intergenic variant that is reported to be associated with serum creatine kinase levels (32), were found to be significantly associated with coronary plaque rupture in a recessive model (odds ratio [OR] = 2.04, 95% CI, 1.01–4.09, $P < 0.05$) (Figure 7E, Table 2, and see Supplemental Table 1 for patients' characteristics). (Individuals of European descent have a lower prevalence of this SNP, with a minor allele frequency [MAF] of 11%–12% vs. approximately 50% for individuals of African American descent.) To further examine the effect of the homozygous minor alleles in ruptured coronary plaques, 47 individuals with plaque rupture carrying homozygous major versus minor allele genotypes were selected for microvasculature analysis. Measurement of microvessel density at the rupture site of the coronary artery revealed that subjects with a homozygous minor allele genotype (GG genotype carriers) had significantly more angiogenesis than did those with a homozygous major allele genotype (AA genotype carriers) (Figure 7F). We found that the traditional cardiovascular risk factors were not different between these 2 groups (see patients' characteristics

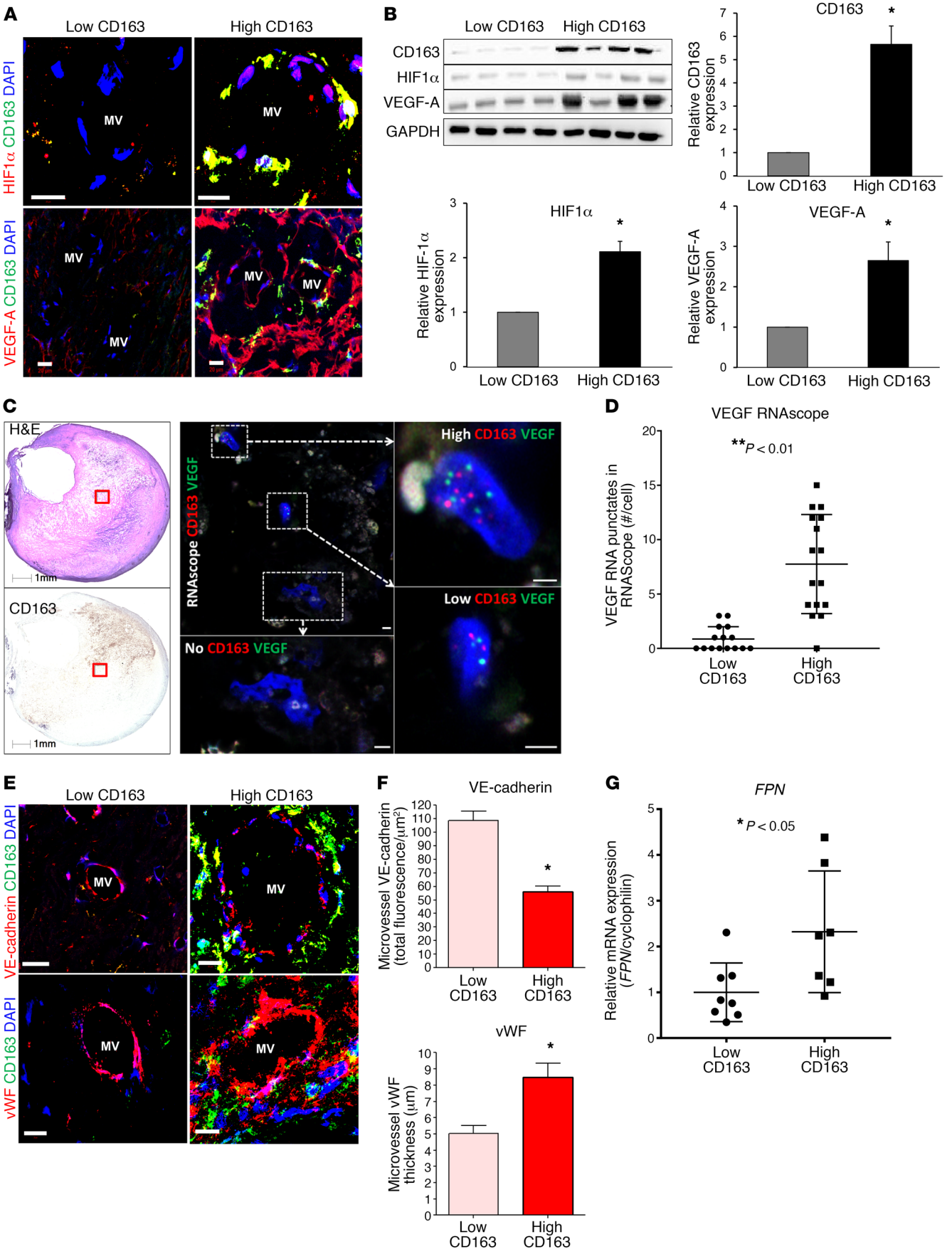
A
Low CD163
High CD163
HIF1α CD163 DAPI
VEGF-A CD163 DAPI
MV
B
Low CD163
High CD163
CD163
HIF1α
VEGF-A
GAPDH
Relative CD163 expression
Relative HIF-1α expression
Relative VEGF-A expression
C
H&E
1mm
CD163
RNAscope CD163 VEGF
High CD163 VEGF
Low CD163 VEGF
No CD163 VEGF
D
VEGF RNAscope
**P < 0.01
VEGF RNA punctates in RNAScope (#/cell)
Low CD163
High CD163
E
VE-cadherin CD163 DAPI
vWF CD163 DAPI
F
VE-cadherin
Microvessel VE-cadherin (total fluorescence/μm²)
vWF
Microvessel vWF thickness (μm)
G
FPN
*P < 0.05
Relative mRNA expression (FPN/cyclophilin)

Figure 2. Alternative CD163⁺ macrophages are associated with intraplaque angiogenesis and vascular permeability and express HIF1α and VEGF-A. Human plaques from CEA specimens were analyzed by histology and immunofluorescence. Images were acquired by confocal microscopy using ×40 (**A** and **E**) or ×60 (**C**, RNAscope) objectives, with optical slicing in the *z* axis. (**A**) Representative microvessels (MV) from low and high CD163 areas (green) dual immunostained for HIF1α and VEGF-A (red channels). Scale bars: 20 μm. (**B**) immunoblotting for CD163, HIF1α, VEGF-A, and GAPDH of protein extracted from human atheroma expressing high or low levels of CD163 (*n* = 4 samples each). Bar graphs show quantitation of densitometry for the indicated proteins. (**C**) RNAscope ISH analysis using CD163 (red) and VEGF (green) probes on human carotid plaques. H&E and CD163 immunohistochemically stained images of human carotid plaques are shown on the left to indicate the areas (red boxes) of RNAscope ISH images of CD163 and VEGF, shown on the right. Scale bars: 1 mm (H&E- and immunostained images) and 2 μm (ISH). (**D**) Quantitative graph of VEGF RNA punctate counts in macrophages with low (<1–4 punctates) or high (≥5 punctates) CD163 expression (total of 3 plaques used for data collection, with 5 to 6 areas per plaque). (**E**) representative microvessels from low and high CD163 areas (green) dual immunostained for VE-cadherin and vWF (red channels). Note that VE-cadherin expression is located exclusively along the interendothelial contacts. The fluorescence signal for VE-cadherin appeared to be attenuated in a microvessel surrounded by CD163⁺ macrophages, with diffuse expression of vWF antigen, suggestive of leaky endothelial junctions. Scale bars: 20 μm. (**F**) Bar graphs show quantification of fluorescence signals for VE-cadherin and vWF in low and high CD163 areas (multiple areas from a total of 10 plaques per group were examined; see Methods). (**G**) Laser capture microdissection and qPCR analysis of FPN expression in low CD163⁺ and high CD163⁺ macrophage areas (*n* = 15 plaques sampled). Results are presented as the mean ± SEM (**B** and **F**) or the mean ± SD (**D** and **G**). (**B** and **F**) $^*P < 0.05$, by 2-sided Student's *t* test. (**D** and **G**) $P < 0.01$ and $P < 0.05$, by 2-sided Student's *t* test.

in Supplemental Table 2). Significantly higher levels of *CD163* mRNA were found in the ruptured coronary arteries of the homozygous G allele carriers (Figure 7G). To confirm the significance of rs7136716 in a large, independent cohort, 3,364 participants of African American ancestry from the Atherosclerosis Risk in Communities (ARIC) study were examined for genotypic and phenotypic data. A total of 3,225 subjects free of prevalent coronary heart disease (CHD) at baseline were included in the analysis. Baseline characteristics for the 3,225 participants with genotypic data and free of prevalent CHD at baseline are shown in Supplemental Table 3. A total of 1,311 incident CHD events occurred during follow-up, of which 338 were myocardial infarctions (MI). The mean follow-up period was 18.4 years for MI patients and 12.8 years for CHD patients. The rs7136716 variant indicated significant associations with both incident MI and incident CHD (hazard ratio = 1.21, 95% CI, 1.05–1.40, $P = 0.0054$, and hazard ratio = 1.20, 95% CI, 1.05–1.35, $P = 0.0026$, respectively) (Figure 7H). Together, these human data suggest that the rs7136716 variant in CD163 is a possible risk factor of CHD in patients of African American ancestry.

Discussion

IPH and macrophages play important roles in the development of advanced atherosclerotic plaques. However, our understanding of the mechanisms by which they do so remains incomplete. Within this context, it seems natural to assume that within areas of IPH, the release of free Hb and its uptake by macrophages would protect against its deleterious effects by suppressing iron-derived toxicity. Indeed, previous work by our group and others has demonstrated that Hb is an important stimulus for alternative macrophage differentiation into a non–foam cell phenotype with antioxidative properties and reduced inflammatory cytokine expression that some have termed atheroprotective (6, 12, 13). Here, we show the unexpected but important finding that, within M(Hb) macrophages, relative iron deprivation inhibited the function of PHD2, leading to increased HIF1α-mediated angiogenesis, vascular permeability, and microvascular inflammation — features seen in advanced atherosclerotic plaques. These results suggest that the macrophage inflammatory response to hemorrhage actually promotes plaque destabilization by initiating a vicious cycle that likely leads to further intraplaque bleeding, inflammatory cell recruitment, and necrotic core expansion (Figure 8). Consistent with this, mice with combined deletion of *CD163* and *ApoE* had significantly reduced plaque progression as compared with *ApoE*-deficient mice. Our findings highlight a nonlipid-driven mechanism by which alternative macrophages promote human plaque progression and indicate that HIF1α/VEGF-A is an important target for antiatherosclerotic therapies.

Wartman proposed more than 75 years ago that IPH might be a major contributor to the progression of coronary artery lesions (33). We and others have previously shown that IPH is a critical event in atherogenesis that fundamentally alters the plaque microenvironment by increasing the content of red cell membrane–derived free cholesterol causing necrotic core expansion and plaque progression (8). Studies involving the injection of silicon polymer into atherosclerotic human coronary arteries have revealed an elaborate microvascular network extending from the adventitia through the media and into the thickened intima (34). IPH is believed to arise from the disruption of thin-walled microvessels that are lined by discontinuous endothelium without supporting smooth muscle cells (19). However, the means by which such extensive angiogenesis occurs within intraplaque vessels has remained uncertain.

Table 2. Homozygous carriers of the minor allele of the CD163 SNP rs7136716 versus noncarriers

SNP number	SNP type	Total minor allele frequency (*n* = 346 pts)	Homozygous minor allele in ruptures (*n* = 51 pts)	Homozygous minor allele in nonruptures (*n* = 295 pts)	*P* value
rs7136716	Upstream intergenic	43% (G allele)	14 (27.5%)	46 (15.6%)	0.046

Homozygous carriers of the minor allele of the CD163 SNP rs7136716 versus noncarriers were evaluated in plaque rupture versus nonrupture cases in the CVPath cohort (*n* = 346). pts, patients. The *P* value was determined by Fisher' exact test to examine the association of the genetic variant with the plaque rupture.

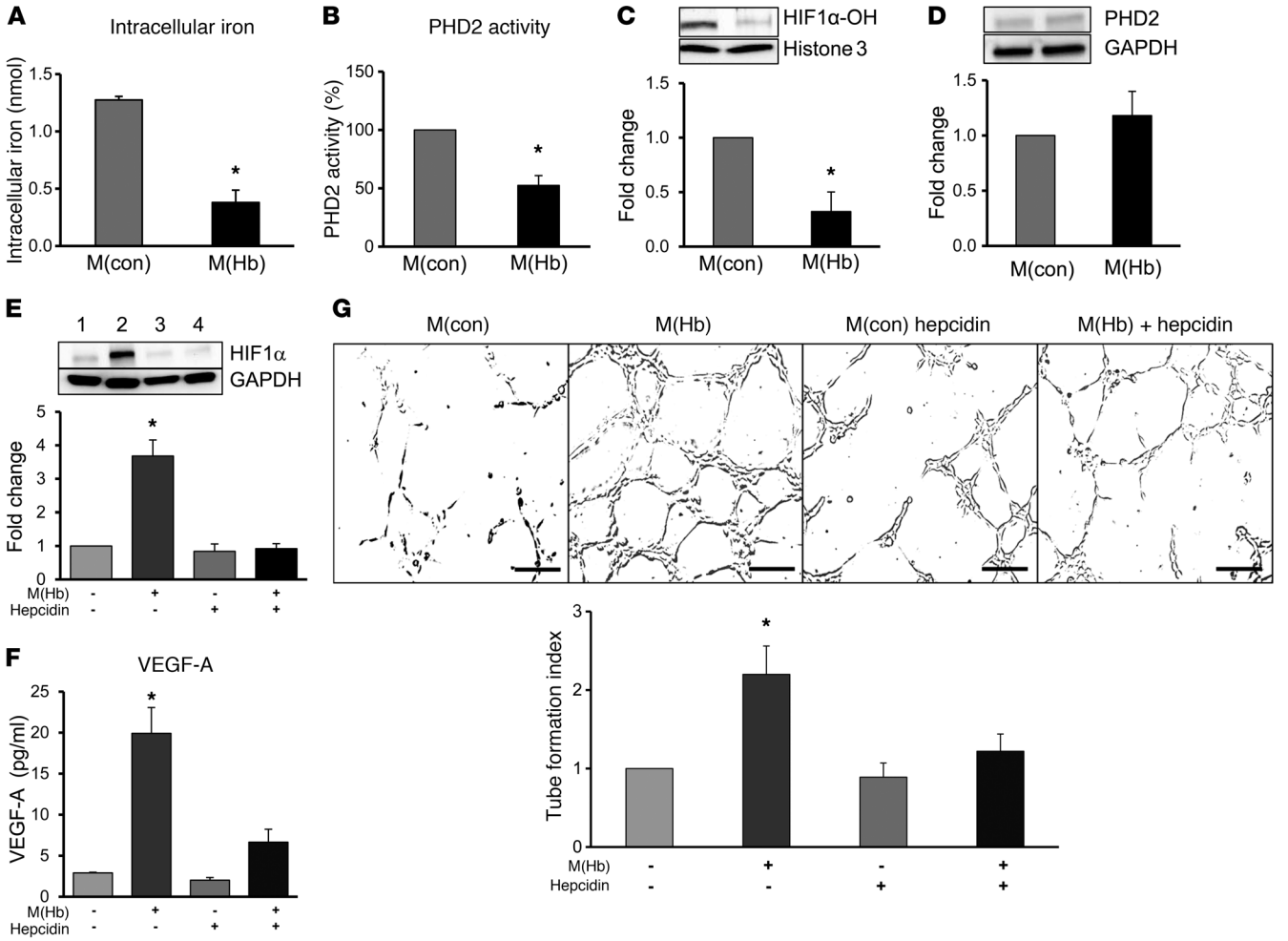

Figure 3. Inhibition of PHDs by relative iron deprivation within M(Hb) macrophages increases HIF1α/VEGF-A signaling and promotes angiogenesis. (**A**) Intracellular free iron levels in control [M(con)] or HH-differentiated [M(Hb)] human macrophages (n = 4 per group). (**B**) PHD2 activity of human macrophages after HH treatment compared with control (n = 5 per group). (**C** and **D**) Immunoblotting of human macrophages (n = 4 per group) with quantitation of densitometry for HIF1α-OH and PHD2. (**E**) Immunoblotting of human macrophages (n = 4 per group) with quantitation of densitometry for HIF-1α. (lane 1: control macrophages; lane 2: HH-stimulated macrophages; lane 3: control macrophages + 700 nM hepcidin; lane 4: HH-stimulated macrophages + 7 00 nM hepcidin). (**F**) ELISA analysis of macrophage supernatants for VEGF-A (n = 5 per group). As in **E**, the bars represent, from left to right: control macrophages, HH-stimulated macrophages, control macrophages plus 700 nM hepcidin, and HH-stimulated macrophages plus 700 nM hepcidin. (**G**) Tube formation assays of HAECs with macrophage supernatant. Relative tube-forming abilities are shown with representative images on top and quantitated tube-formation index below (n = 5 per group). Scale bars: 200 μm. All error bars indicate the mean ± SEM. Comparisons between 2 groups were conducted using a 2-sided Student's t test. For multiple group comparisons, a 1-way ANOVA was applied. If the variance ratio test (F test) was significant, a more detailed post-hoc analysis of differences between groups was made using a Tukey-Kramer honest significant difference test. *P < 0.05 versus control in **A**–**D** versus other groups in **E**–**G**.

Hypoxia resulting from intimal thickening is thought to be the major cause of plaque angiogenesis. Sluimer et al. previously demonstrated hypoxia in human carotid specimens using the bioreductive agent pimonidazole (35). Hypoxia was strongly correlated with the macrophage marker CD68, angiogenesis, and thrombus in regions of advanced atheroma but was absent in areas of PIT. HIF1α immunoreactivity and mRNA were detected at sites of inflammation, even in areas within a close distance (20–30 μm) from the vessel lumen, well below the diffusion limits of oxygen (100–250 μm). Here, we expand upon our knowledge of the mechanisms driving intraplaque angiogenesis to define the cell biology and molecular pathways responsible for these changes. The infiltration of macrophages into plaque areas containing free Hb with subsequent uptake via CD163 results in significant changes in macrophage iron metabolism that lead to relative intracellular iron deprivation and inhibition of iron-dependent PHDs. This causes an accumulation of HIF1α, which mediates angiogenesis through increased VEGF. While hypoxia may be an additional and important factor, our data clearly demonstrate that Hb intake by human macrophages under conditions of normoxia drives their differentiation into proangiogenic cells. Further supporting our contention is the fact that genetic deletion of CD163, a macrophage-specific protein, resulted in a significant reduction in angiogenesis (P < 0.05, Figure 5, H and I) and plaque progression (P < 0.01, Figure 5, C–G) in our mouse model. Interestingly, a recent study by Marsch and colleagues showed that PHD1-knockout mice have a metabolic phenotype that is generally deemed protective for cardiovascular disease (36). Additional

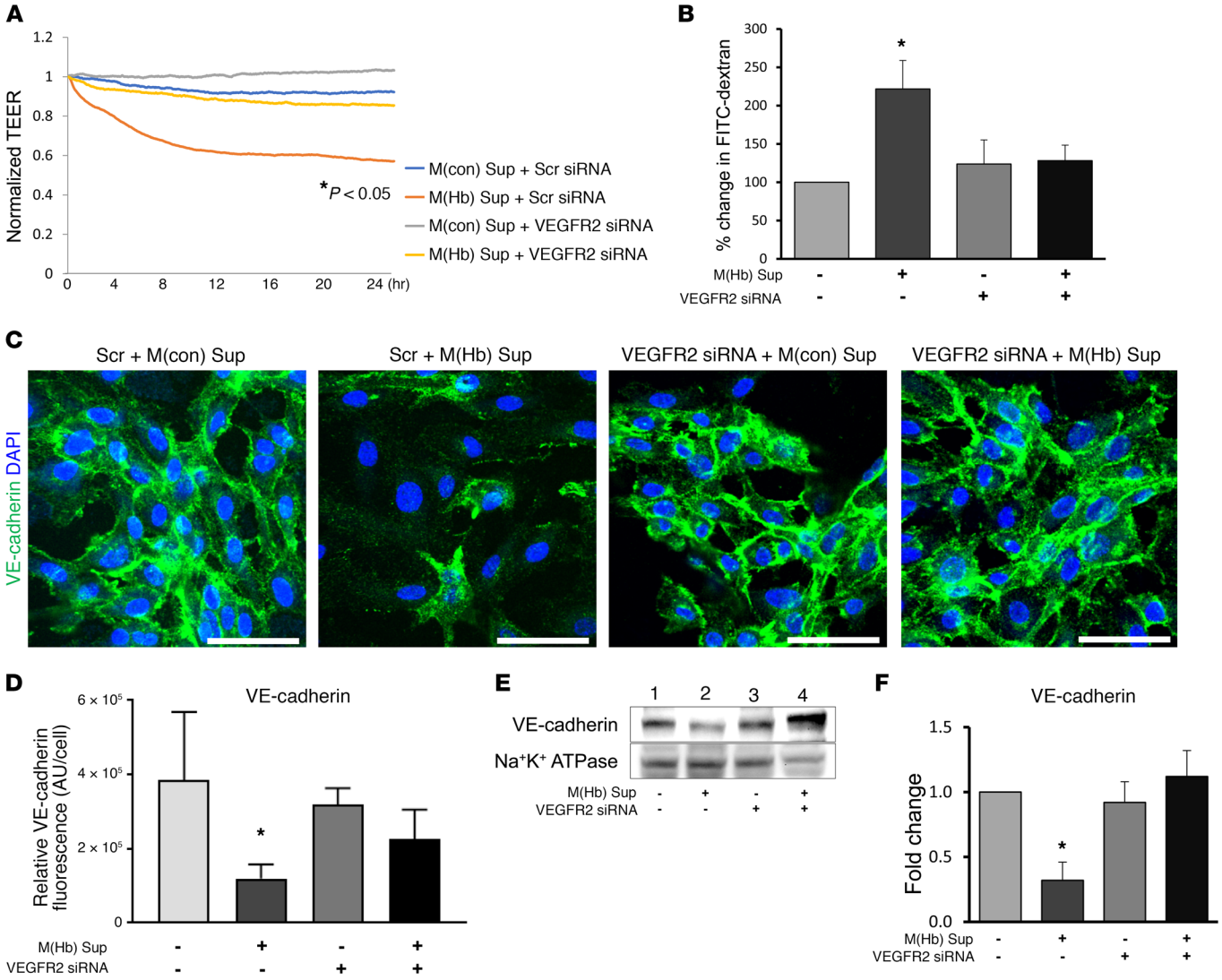

Figure 4. M(Hb) macrophages promote vascular permeability via VEGF-A/VEGFR2 signaling. (**A**) TEER measurements after treatment of scramble siRNA–(Scr) or VEGFR2 siRNA–transfected HAECs with supernatant from control macrophages [M(con)] or HH-differentiated [M(Hb)] macrophages. The relative TEER compared with control is shown (n = 4 per group). (**B**) FITC-dextran permeability in scramble siRNA– or VEGFR2 siRNA–transfected HAECs treated with control or HH-differentiated macrophage supernatants. Percentage change of FITC-dextran compared with control (n = 4 per group). (**C**) Immunofluorescence imaging of scramble siRNA– or VEGFR2 siRNA–transfected HAECs treated with control or HH-differentiated macrophage supernatants for VE-cadherin (green) and DAPI (blue) (original magnification, ×60). Scale bar: 50 μm. Note the loss of plasma membrane VE-cadherin in endothelial cells treated with M(Hb) supernatants versus M(con) supernatants and the restoration of membrane VE-cadherin in endothelial cells transfected with VEGFR2 siRNA and treated with M(Hb) supernatants. (**D**) Quantitation of plasma membrane VE-cadherin in the experiment shown in **C** (n = 10 per group). (**E**) Immunoblot of the membrane fraction from scramble siRNA– or VEGFR2 siRNA–transfected HAECs treated with control or HH-differentiated macrophage supernatants, with quantitation of densitometry for VE-cadherin (n = 4 per group). (**F**) Quantitation of plasma membrane VE-cadherin in the experiment shown in **E**. All error bars indicate the mean ± SEM. *P < 0.05 versus other groups. For multiple group comparisons, a 1-way ANOVA was applied. If the variance ratio test (F test) was significant, a more detailed post-hoc analysis of differences between groups was done using a Tukey-Kramer honest significant difference test.

studies are needed to understand the differential function of each PHD isoform in the context of atherosclerosis.

Earlier work by our group and that of others has shown that microvessels within advanced atherosclerotic plaques exhibit compromised endothelial cell morphology and integrity characterized by loss of VE-cadherin (19, 20). However, the causes for increased vascular permeability with human atherosclerosis have remained unclear. Bobryshev and colleagues previously reported that while VE-cadherin was readily detectable in areas of human intraplaque vessels lacking inflammatory cells, it was irregularly distributed in vessels surrounded by large numbers of inflammatory cells (20). Our data indicate that VEGF-A secreted from CD163$^+$ macrophages is the cause of these abnormalities. Supernatants from HH-differentiated M(Hb) macrophages caused significant increases in vascular permeability (P < 0.05, Figure 4, A and B) and VE-cadherin internalization (P < 0.05, Figure 4, C–F) in cultured endothelial cells but not in the presence of endothelial cells treated with VEFGR2 siRNA. Moreover, similar experiments demonstrated increases in endothelial VCAM, which was inhibited in the presence of VEGFR2 siRNA. Additionally, in *ApoE*$^{-/-}$

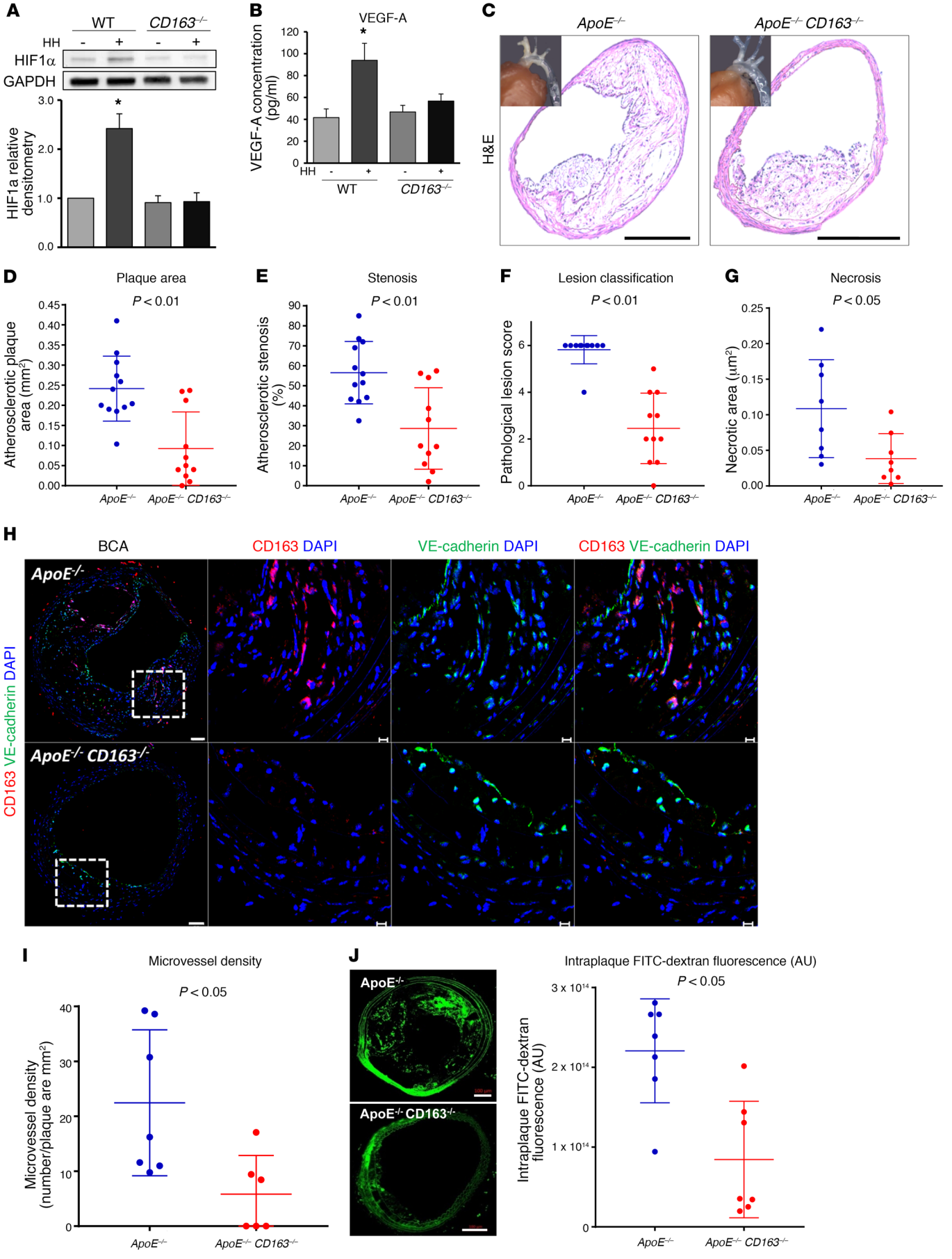
A
WT
CD163-/-
HH
HIF1α
GAPDH
HIF1a relative densitometry
B
VEGF-A
VEGF-A concentration (pg/ml)
C
ApoE-/-
ApoE-/- CD163-/-
H&E
D
Plaque area
P < 0.01
Atherosclerotic plaque area (mm2)
E
Stenosis
P < 0.01
Atherosclerotic stenosis (%)
F
Lesion classification
P < 0.01
Pathological lesion score
G
Necrosis
P < 0.05
Necrotic area (μm2)
H
BCA
CD163 DAPI
VE-cadherin DAPI
CD163 VE-cadherin DAPI
CD163 VE-cadherin DAPI
I
Microvessel density
P < 0.05
Microvessel density (number/plaque are mm2)
J
Intraplaque FITC-dextran fluorescence (AU)
P < 0.05
Intraplaque FITC-dextran fluorescence (AU)

Figure 5. Deletion of CD163 in mice reduces intraplaque neovascularization and plaque progression. (**A**) Immunoblotting of mouse macrophages with quantitation of densitometry for HIF1α in macrophages isolated from WT or *CD163*$^{-/-}$ mice stimulated with Hb (n = 4 per group). (**B**) Analysis of macrophage supernatant for VEGF-A by ELISA (n = 4 per group). (1: WT macrophages, 2: Hb-stimulated WT macrophages, 3: *CD163*$^{-/-}$ macrophages, 4: Hb-stimulated *CD163*$^{-/-}$ macrophages). (**C**) Representative H&E staining of BCA plaque with a of gross inset photograph of the aortic arch from 1-year-old *ApoE*$^{-/-}$ and *ApoE*$^{-/-}$ *CD163*$^{-/-}$ mice. Scale bars: 100 μm. (**D**–**G**) Quantitative measurements of lesion size, percentage of stenosis, lesion pathological scores, and necrotic areas in the BCA plaque (n = 8–12 per group). (**H**) Representative immunofluorescence confocal microscopic images of BCA plaque stained with VE-cadherin (green), CD163 (red), and DAPI (blue). Scale bars: 50 μm and 10 μm (enlarged images of boxed areas on the left). (**I**) Microvessel density quantification calculated by the number of microvessels per plaque area identified by VE-cadherin immunofluorescence confocal microscopy (n = 6–7 per group). (**J**) Representative immunofluorescence confocal microscopic images of intraplaque FITC-dextran (green) as a marker for permeability. Scale bars: 100 μm. Total intraplaque FITC fluorescence was quantified from confocal images of BCA plaques perfused with FITC-dextran to determine permeability (n = 7 per group). Bars and plots indicate the mean ± SEM (**A** and **B**) or the mean ± SD (**D**–**G**, **I**, and **J**). (**A** and **B**) *P < 0.05 versus other groups, by 1-way ANOVA , and, if the ratio test (F test) was significant, a more detailed post-hoc analysis of differences between groups was performed using a Tukey-Kramer honest significant difference test. (**D**–**G**, **I**, and **J**) P < 0.01 and P < 0.05, by 2-sided Student's t test.

mice, a VEGF-blocking antibody not only decreased intraplaque endothelial VCAM expression but also inhibited monocyte recruitment. Similarly, human plaque microvessels surrounded by CD163$^+$ cells showed abnormalities in VE-cadherin and extravasation of vWF, unlike those located away from CD163$^+$ cells. Deletion of *CD163* in mice reduced plaque permeability, microvessel quantity, microvascular inflammation, inflammatory cell recruitment, and plaque progression. These data strongly suggest that macrophage-secreted VEGF-A is an important factor increasing endothelial permeability within human intraplaque vessels.

While the macrophages inflammatory response in areas of IPH is essential for controlling the toxic effect of free iron derived from erythrocytes, the resultant proangiogenic changes in macrophage function are almost certainly pathogenic within the context of atherosclerosis. Small amounts of intimal angiogenesis and bleeding might be made worse by the resultant inflammatory response. Clinical studies using serial carotid MRI to detect IPH in humans with carotid artery disease have shown that IPH has long-standing deleterious effects on plaque growth that remain detectable for years after the initial bleeding event (37). Although not specifically explored by us, it is likely that the macrophage response to hemorrhage shown here is similar to that for other diseases in which hemorrhage (i.e., tumors, diabetic retinopathy, and macular degeneration) plays an important role.

We previously hypothesized that antiangiogenic therapies using VEGF-A inhibitors might be important for the normalization of plaque vasculature and thus limit further risk of IPH and necrotic core expansion (7). By reducing vessel growth, permeability, and leukocyte recruitment, such therapies might be able to limit the initial effects of IPH. Our data suggest that in patients with IPH identified via MRI or perhaps by molecular imaging of M(Hb) macrophages, local anti–VEGF-A therapies might be useful in halting plaque progression. Given the known side effects of proteinuria, hypertension, and thromboembolism, the risks of systemic anti-VEGF therapies might not be justified (38).

We would be remiss if we did not briefly discuss the limitations of this study. Surgical CEA specimens involve a certain selection bias of surgical manipulation, in that these findings may not be representative of humans with IPH who do not undergo endarterectomy. The anti-CD163 antibodies used in this study could also potentially detect soluble CD163 in the specimens, but we believe this is unlikely, given that the specimens were perfusion fixed and that the vast majority of CD163 expression was associated with nucleated cells. Moreover, given the observational nature of human pathology studies, it remains uncertain as to what extent the intimal angiogenesis and vascular permeability seen in the samples examined can be attributed to M(Hb) cells as opposed to other causes. Last, we focused on local iron and Hb release at sites of IPH; however, there may be other important potential contributors to plaque progression not explored here, including lesional cytokine production by CD163$^+$ macrophages and local thrombin generation with consequent changes in cellular functions induced by protease-activated receptor action. Nonetheless, the in vitro demonstrations of these effects in cultured endothelial cells under normoxic conditions and in a CD163-deficient mouse model of IPH lend further support to our conclusions. In addition, while we identified a relationship between a human CD163 polymorphism (i.e. rs7136716) and its relationship to increased risk of MI and CHD in African Americans, this SNP has not been previously related to the risk of CHD in larger GWAS studies, which have mostly been conducted in individuals of European and Asian descent (39). This might be due to the low frequency of homozygous minor allele carriers in European populations (<1%) in contrast to its expression in other ethnic groups (20%–30%). Moreover, because the location of this variant is 30 kbp upstream of the *CD163* promoter, its function in relationship to CD163 remains unknown and difficult to determine. Nonetheless, our data showing greater plaque angiogenesis and CD163 expression in subjects with 2 copies of the G-allele suggest a functional role for this SNP with regard to CD163.

In conclusion, our study demonstrates for the first time to our knowledge that a specific alternative macrophage subset driven by uptake of Hb promotes intimal angiogenesis, vascular permeability, and plaque inflammation, features that probably promote plaque progression. Our data also reveal the molecular mechanisms underlying these effects and pinpoint the HIF1α/VEGF-A system as a potential target for antiatherosclerotic therapies.

Methods

Human carotid specimens. Human carotid plaques removed from patients eligible for surgical CEA and pathological specimens of coronary artery samples were selected from the CVPath Registry (18). All plaques were identified according to a modified American Heart Association classification (40). Thirty-eight human carotid plaques removed from patients eligible for surgical CEA, in which the carotid plaque (common and internal carotid artery plaque) was removed in an undisturbed manner, were selected from the CVPath Registry of sixty cases. Indications for surgery were ipsilateral symptoms involving transient ischemic attack or stroke in the previous 6 months or signifi-

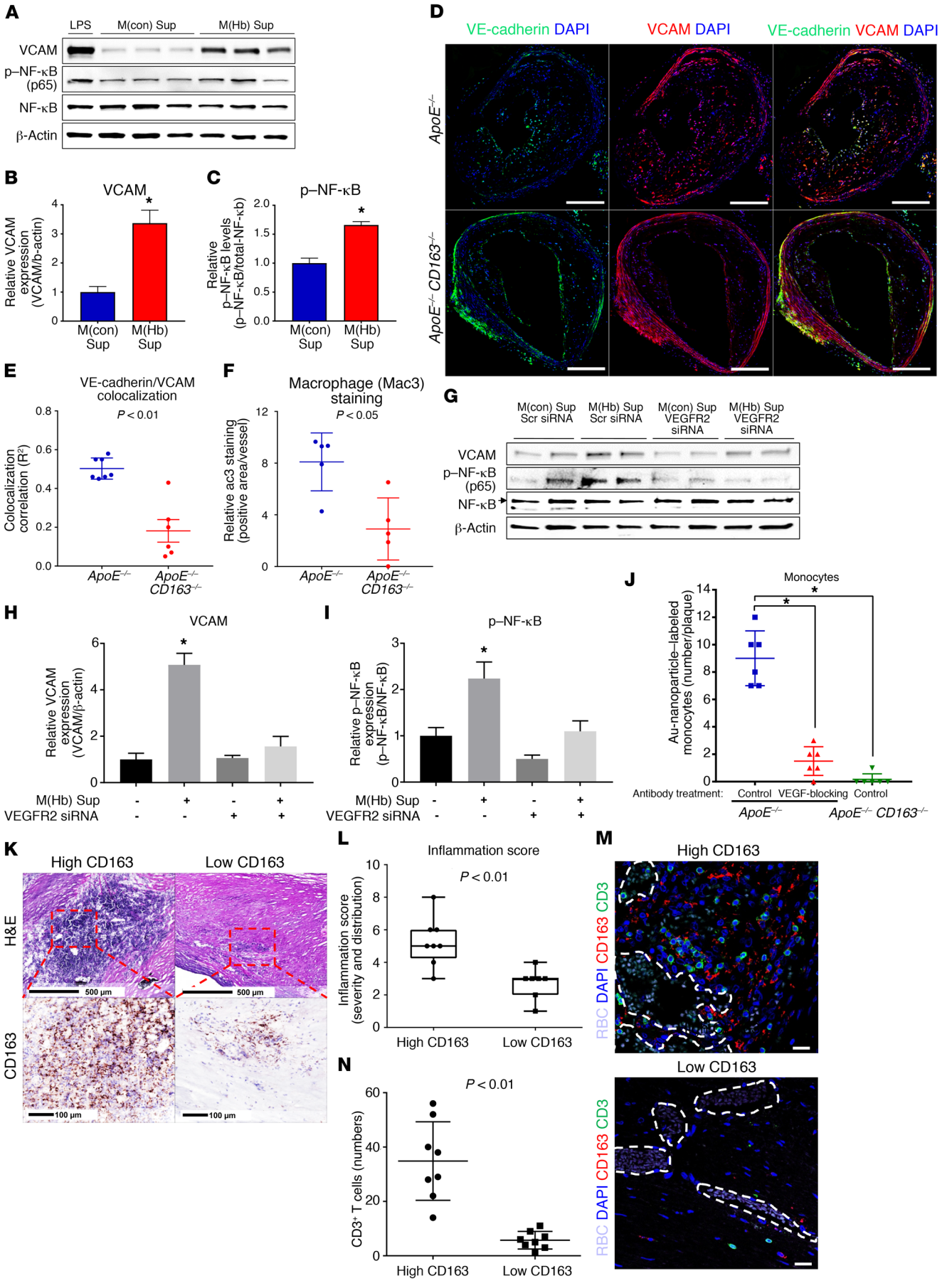
A
LPS
M(con) Sup
M(Hb) Sup
VCAM
p–NF-κB (p65)
NF-κB
β-Actin
B
VCAM
Relative VCAM expression (VCAM/b-actin)
M(con) Sup
M(Hb) Sup
C
p–NF-κB
Relative p–NF-κB levels (p–NF-κB/total-NF-κb)
D
VE-cadherin DAPI
VCAM DAPI
VE-cadherin VCAM DAPI
ApoE−/−
ApoE−/− CD163−/−
E
VE-cadherin/VCAM colocalization
P < 0.01
Colocalization correlation (R²)
F
Macrophage (Mac3) staining
P < 0.05
Relative ac3 staining (positive area/vessel)
G
M(con) Sup Scr siRNA
M(Hb) Sup Scr siRNA
M(con) Sup VEGFR2 siRNA
M(Hb) Sup VEGFR2 siRNA
VCAM
p–NF-κB (p65)
NF-κB
β-Actin
H
VCAM
Relative VCAM expression (VCAM/β-actin)
M(Hb) Sup
VEGFR2 siRNA
I
p–NF-κB
Relative p–NF-κB expression (p–NF-κB/NF-κB)
J
Monocytes
Au-nanoparticle–labeled monocytes (number/plaque)
Antibody treatment:
Control
VEGF-blocking
Control
K
High CD163
Low CD163
H&E
CD163
500 μm
100 μm
L
Inflammation score
P < 0.01
Inflammation score (severity and distribution)
N
P < 0.01
CD3+ T cells (numbers)
M
High CD163
Low CD163
RBC DAPI CD163 CD3

Figure 6. CD163⁺ macrophages increase intraplaque endothelial VCAM and leukocyte recruitment via VEGF. Activation of VCAM and NF-κB in HAECs (**A**–**J**) and association of high CD163⁺ macrophages and inflammation in human atherosclerotic lesions (**K**–**N**). In **A**–**C**, HAECs were incubated with culture media supernatants collected from human macrophages differentiated in HH [M(Hb) Sup] or control media [M(con) Sup] overnight. The expression of VCAM, p-p65 (p–NF-κB), and total NF-κB was measured by immunoblotting. LPS (100 ng/ml) was used as a positive control (n = 4 per group). (**D**) Immunostaining for VE-cadherin (green) and VCAM (red) in BCA plaques from 1-year-old *ApoE*$^{-/-}$ and *ApoE*$^{-/-}$ *CD163*$^{-/-}$ mice. Scale bars: 100 μm. (**E**) The colocalization of VE-cadherin and VCAM in confocal microscopic images was analyzed for correlation coefficiency (n = 6–7 per group). (**F**) Total macrophage content in BCA plaques as described in **H** was analyzed using macrophage marker Mac3 immunohistochemical staining (n = 5 per group). (**G**–**I**) Cells were transfected with VEGFR2 siRNA for 48 hours before incubation with culture media supernatants from macrophages differentiated with HH or control media. The expression of VCAM, ICAM, p-p65 (p–NF-κB), and total NF-κB was measured by immunoblotting (n = 4 per group). Scr siRNA, scrambled siRNA. (**J**) Monocyte infiltration into BCA plaques from 6- to 8-month-old mice after a 4-week treatment with a control or VEGF-blocking antibody. Monocyte tracing was performed by injecting Au-nanoparticle–labeled monocytes, and labeled monocytes were counted on histological images (n = 6 per group). (**K**) Representative images of H&E and CD163 immunohistochemical staining showing high CD163 and low CD163 areas. Scale bars: 500 μm and 100 μm. (**L**) Areas of high and low expression of CD163⁺ macrophages in human atherosclerotic plaques were scored for inflammation (n = 7–8 per group). (**M**) CD163⁺ macrophages and CD3⁺ T cells were detected surrounding microvessels in high CD163 areas (white dashed lines show microvessels). Scale bars: 20 μm. (**N**) Quantitation of CD3⁺ T cells in high and low CD163⁺ macrophages surrounding intraplaque microvessels (n = 8 per group). Data represent the mean ± SEM (**B**, **C**, and **H**–**J**), the mean ± SD (**E**, **F**, **J**, and **N**), or the median for the box and whisker plot (**L**). (**H**–**J**) *P < 0.05, by 1-way ANOVA, and, if the variance ratio test (F test) was significant, a more detailed post-hoc analysis of differences between groups was performed using a Tukey-Kramer honest significant difference test. (**B** and **C**) *P < 0.05, by 2-sided Student's t test. (**E**, **F**, and **N**) P < 0.01 and P 0.05, by 2-sided Student's t test. (**L**) P < 0.01, by Mann-Whitney-Wilcoxon test.

cant carotid stenosis (>70%) measured by duplex ultrasound. In total, there were 18 symptomatic cases and 20 asymptomatic cases. At surgery, the carotid tissue was chilled immediately after excision and then promptly frozen at –80°C and shipped to the CVPath Institute. The CEA specimen was partially thawed and frozen in OCT (Miles Inc.). Cryosections were prepared using a Hacker Bright OTF/HS microtome cryostat equipped with a tungsten carbide knife with an installed CryoJane (Leica Microsystems). The CryoJane Tape-Transfer System improves cryosectioning outcomes on glass slides, particularly for the heavily calcified tissues common to carotid plaques (41). The frozen tissue was step sectioned at 10-μm thickness, 15 to 20 serial sections for staining were collected on glass slides, and adjacent frozen sections of 1.0 to 1.2 mm were collected in plastic tubes and frozen for protein extraction (see below). These steps were repeated until the frozen block was exhausted. This method allowed matching of histological findings with protein analysis. The entire carotid plaque removed at surgery was sampled in this manner.

Lesion classification and selection. Lesion morphology was assessed according to a simplified scheme as previously reported by our laboratory (40). Three sections from each carotid plaque were selected for morphometric analysis, the lesions with the plaque rupture site or ulceration or the most severely narrowed segment were used as the culprit site, and lesions flanking plaques) located 1.2 mm above or below the presenting lesion were also assessed by IHC. Thirty-eight specimens containing culprit segments along with proximal and distal flanking segments were available for analysis and assessed for plaque morphology. A total of 114 plaques (38 culprit, 38 proximal flanking, and 38 distal flanking plaques) were classified, of which 38 were fibroatheromas, 20 were healed plaque ruptures, 14 were fibrocalcific lesions, 11 were plaque ruptures, 9 were TCFAs, 7 were calcified nodules, 5 were PITs, 5 were intimal xanthomas, 2 were chronic total occlusions, 2 were fissures, and 1 was a fibrous plaque.

Inflammation scoring. Pathological scoring of plaque inflammation was performed to assess its severity and distribution. Plaque inflammation was regionally assessed using a scoring system accounting for both the severity according to the number of inflammatory cells and the relative distribution based on quadrants. Severity was scored on a scale of 0 to 4: 0–20 inflammatory cells = 0; 21–100 cells = 1; 101–200 cells = 2; 201–400 = 3; and more than 400 cells = 4. Distribution was also scored on a scale of 0 to 4: 0–45 degrees = 0; 45–90 degrees = 1; 90–180 degrees = 2; 180–270 degrees = 3; and 270–360 degrees = 4. The overall inflammation score was drawn from the scoring matrix (Supplemental Table 4). Inflammatory cells (macrophages and T cells) were identified on H&E staining on the basis of their characteristic appearance. Scoring was confirmed by a pathologist (R. Virmani).

Immunohistochemical and immunofluorescence staining. Cryosections were stained using both H&E and Movat pentachrome stains. Areas of foam cell macrophages and M(Hb) macrophage were identified with CD68 and CD163 immunohistochemical staining, respectively, as previously reported (6). The ratio of CD163 to CD68 staining was analyzed, and ratios below 0.20 were considered low CD163 plaque areas, while those above 0.70 were considered high CD163 plaque areas. Ten plaque samples contained high CD163/CD68 areas, while ten plaques contained low CD163/CD68 areas and were collectively chosen for further analysis. Five to six samples each from the plaques with low and high CD163 areas were selected for immunoblotting to detect CD163, HIF1α, and VEGF-A expression in the plaque. Negative control plaques that were low in both CD68 and CD163 showed no HIF1α or VEGF-A expression by immunoblotting (data not shown). Ten plaques were selected from the low and high CD163 area samples for quantitation of angiogenesis. Microvessel numbers were assessed following immunohistochemical staining for anti-CD31 and anti-vWF.

Immunofluorescence staining for CD163/vWF, CD68/vWF, CD163/HIF1α, CD163/VEGF-A, CD163/VE-cadherin, VE-cadherin/VCAM, and CD163/CD3 was carried out on cryosections or formalin-fixed, paraffin-embedded sections. The frozen sections were fixed in cold acetone for 10 minutes, with further exposure to 0.15% H_2O_2 for 20 minutes. The sections were treated with Dako protein block (catalog X0909) for 10 minutes before incubation with primary antibodies against CD163 (Santa Cruz Biotechnology, catalog sc-20066, clone GHI/61, dilution 1:200, overnight at 4°C); CD68 (Dako, clone Kp1, dilution 1:800, 1 hour); vWF (Strategic BioSolutions, S4003GND1, dilution 1:2,000, 1 hour); HIF1α (Novus Biologicals, NB100-105, dilution 1:40, 1 hour); VEGF-A (BioGenex, PU483-UP, dilution 1:40, overnight); VE-cadherin (R&D Systems, AF1002, dilution 1:100, and BD Biosciences, 555661, dilution 1:400, overnight); CD3 (Roche, 790-4341, prediluted); and VCAM (Abcam, ab134047, dilution 1:100). Antibody detection included biotinylated goat anti-rabbit, horse anti-mouse, and rabbit anti-goat (Vector Laboratories,

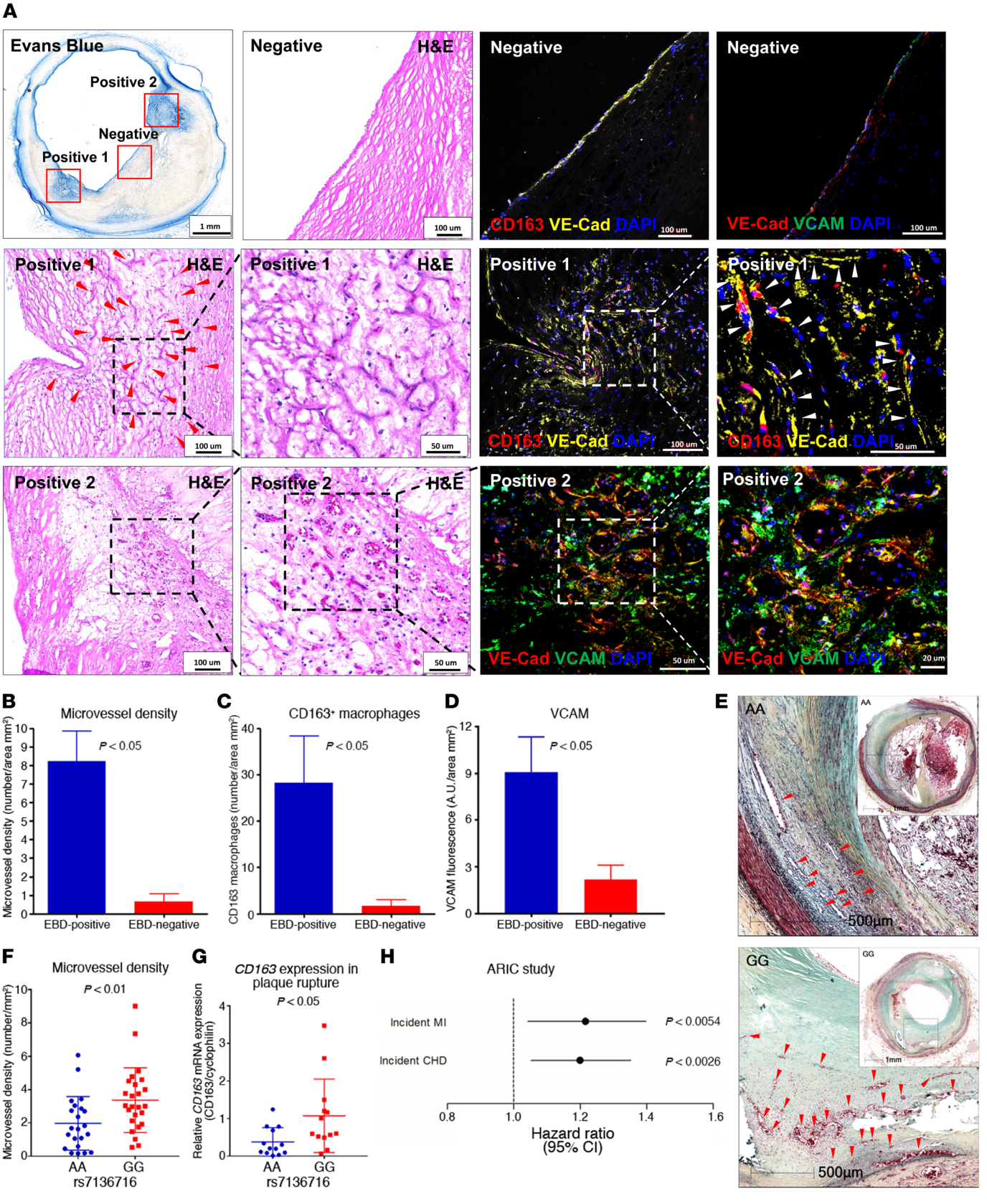
A
Evans Blue
Positive 2
Negative
Positive 1
1 mm
Negative
H&E
100 um
Negative
CD163 VE-Cad DAPI
100 um
Negative
VE-Cad VCAM DAPI
100 um
Positive 1
H&E
100 um
Positive 1
H&E
50 um
Positive 1
CD163 VE-Cad DAPI
100 um
Positive 1
CD163 VE-Cad DAPI
50 um
Positive 2
H&E
100 um
Positive 2
H&E
50 um
Positive 2
VE-Cad VCAM DAPI
50 um
Positive 2
VE-Cad VCAM DAPI
20 um
B
Microvessel density
P < 0.05
Microvessel density (number/area mm²)
EBD-positive
EBD-negative
C
CD163⁺ macrophages
P < 0.05
CD163 macrophages (number/area mm²)
EBD-positive
EBD-negative
D
VCAM
P < 0.05
VCAM fluorescence (A.U./area mm²)
EBD-positive
EBD-negative
E
AA
500μm
GG
500μm
F
Microvessel density
P < 0.01
Microvessel density (number/mm²)
AA
GG
rs7136716
G
CD163 expression in plaque rupture
P < 0.05
Relative CD163 mRNA expression (CD163/cyclophilin)
AA
GG
rs7136716
H
ARIC study
Incident MI
P < 0.0054
Incident CHD
P < 0.0026
0.8
1.0
1.2
1.4
1.6
Hazard ratio (95% CI)

Figure 7. CD163⁺ macrophages are associated with increased angiogenesis and microvessel permeability in human coronary artery plaques. (**A**–**D**) Human coronary artery microvessel permeability was assessed by EBD perfusion. (**A**) Representative images of EBD-perfused human coronary arteries, H&E-stained images, and confocal immunofluorescence images of CD163 (red) and VE-cadherin (yellow) or VE-cadherin (red) and VCAM (green) in an EBD-negative area (top row), EBD-positive area 1 (middle row), and EBD-positive area 2 (bottom row). Positive areas 1 and 2 are shown in progressively higher-magnification H&E-stained images from left to right in the second and third rows. Red and white arrowheads point to microvessels. Confocal images of the EBD-negative areas for CD163/VE-cadherin and VE-cadherin/VCAM are shown in the top row of columns 3 and 4, respectively, while the positive area 1 is shown for CD163/VE-cadherin in the middle rows of columns 3 and 4 (higher-magnification image on the right), and positive area 2 is shown for VE-cadherin/VCAM in the bottom of row of columns 3 and 4 (higher-magnification image on the right). (**B**–**D**) Quantification of microvessel density, CD163⁺ macrophages, and VCAM in an EBD-positive area versus an EBD-negative area (n = 6–8 per group). (**E**) The SNP rs7136716 was associated with human coronary artery atherosclerotic plaque rupture and risk of coronary artery disease. See Table 2 for SNP analysis of the CVPath cohort. Representative images show ruptured plaques in human coronary arteries from subjects with the rs7136717 AA genotype versus the those with the GG genotype. Scale bars: 500 μm. Arrowheads point to microvessels. (**F**) Microvessel density per plaque area at the ruptured coronary artery plaque site from individuals with 0 copies (AA genotype, n = 22) versus 2 copies of the minor allele (GG genotype, n = 25) who died of plaque rupture. (**G**) Relative *CD163* mRNA expression in ruptured coronary artery plaques from AA versus GG genotype groups as measured by qPCR (n = 13 per group). (**H**) Cox proportional hazards ratio assessment for the association of the genetic variant rs7136717 with incident MI and incident CHD in the ARIC cohort (n = 3,225). Data represent the mean ± SD (**B**–**D**, **F**, and **G**) or ORs and 95% CI (**H**). $P < 0.01$ and $P < 0.05$, by 2-sided Student's t test (**B**–**D**, **F**, and **G**). In the ARIC cohort, Cox proportional hazards models were used to examine the association of the genetic variant with incident MI and incident CHD, and the analyses were adjusted for age, sex, ancestry-informative principal components, and study center (**H**).

BA-1000, BA-2000, BA-5000, respectively, at 1:200 dilution) and Alexa Flour 488 and 555 streptavidin (Invitrogen, Thermo Fisher Scientific, S32354 and S32355, respectively, dilution 1:100). The positive and negative controls (sections stained with a secondary antibody only or without any antibody to detect autofluorescence) were included in every staining procedure. The sections were counterstained with DAPI (Invitrogen, Thermo Fisher Scientific, catalog D3571). Images were captured by laser-scanning confocal microscopy (Carl Zeiss, LSM 700, 800, or 880) using ×20 or ×40 objectives with optical slicing in the z axis. Total fluorescence of immunostaining was quantitated using Zen software (Carl Zeiss). Microvessel vWF staining thickness was quantitated by averaging the measurements of multiple points at 5-μm intervals around each microvessel circumference on the HALO platform (Indica Labs).

Human coronary artery samples and EBD permeability assay. Human coronary artery samples were selected from freshly collected autopsy specimens from the CVPath Registry, with a post-modem interval (PMI) cut-off less of than 12 hours and evidence of advanced atherosclerosis based on x-ray images of the heart. EBD (0.5%) solution was prepared and filtered in saline solution containing 5% BSA and then perfused into both the right and left coronary arteries through a mean pressure of approximately 60 mmHg for 15 minute at 37°C. After dye perfusion, samples were further washed with PBS perfusion and fixed by neutral buffered formalin perfusion. Fixed tissue samples were harvested, cut at 2- to 3-mm intervals, and embedded in OCT for frozen sectioning, staining, and histology as well as immunofluorescence analysis. A description of the demographic characteristics of the subjects whose hearts were studied in this experiment is provided in Supplemental Table 5.

RNAscope ISH and laser capture microdissection. In situ detection of CD163 and VEGF transcripts in human atherosclerotic plaques was performed using an RNAscope assay with RNAscope Probe-Hs-CD163-C2 (Advanced Cell Diagnostics, catalog 417061-C2), an RNAscope Probe- Hs-VEGFA (Advanced Cell Diagnostics, catalog 423161), and an RNAscope Fluorescent Multiplex Reagent Kit (Advanced Cell Diagnostics, catalog 320850) following the manufacturer's protocols. Both positive (POLR2A and PPIB) and negative controls were included in the procedure according to the manufacturer's instruction. All slides were digitally scanned with an LSM 800 laser-scanning confocal microscope (Carl Zeiss) using a ×60 objective with Airyscan (Carl Zeiss). Laser capture microdissection was performed as previously described (6).

Human coronary plaque and CD163 SNPs. SNPs from the *CD163* gene were examined in 346 subjects (51 with plaque rupture and 295 with nonruptured plaques) from the CVPath Registry on an Illumina Exome BeadChip array. For further analysis of rs7136716, there were a total 111 subjects with homozygous major AA alleles, 175 with heterozygous AG alleles, and 60 with homozygous minor GG alleles. Evidence of plaque rupture was detected by serial sectioning of culprit plaques as identified by H&E and Movat pentachrome staining. Among the subjects with plaque ruptures, 15 had homozygous major AA alleles, 22 had heterozygous AG alleles, and 14 had homozygous minor GG alleles. The ruptured culprit lesions in coronary arteries were analyzed for intraplaque microvessel density in age- and sex-matched subjects with homozygous major alleles and in subjects with homozygous minor alleles. RNA was extracted from ruptured artery specimens, and CD163 expression levels were measured by quantitative PCR (qPCR) using SYBR Green Master Mix (Life Technologies, Thermo Fisher Scientific).

CHD risk of SNPs in the human cohort. The Atherosclerosis Risk in Communities (ARIC) study is a prospective, population-based cohort study designed to investigate the etiology and predictors of cardiovascular disease and has been described in detail previously (42). Briefly, participants aged 45 to 64 years at baseline were recruited from 4 communities: Forsyth County, North Carolina; Jackson, Mississippi; Minneapolis, Minnesota; and Washington County, Maryland. A total of 15,792 individuals, predominantly of European and African American ancestry, participated in the baseline examination between 1987 and 1989, with 3 additional triennial follow-up examinations and a fifth examination between 2011 and 2013. In the present study, we included only participants of African American ancestry. Human Exome BeadChip, version 1.0 (Illumina), was used to genotype 247,870 exonic variants across the genome, which were called within the context of the Cohorts for Heart and Aging Research in Genomic Epidemiology (CHARGE) consortium as described previously (43, 44). Only genotypes for the genetic variant rs7136716 were used in the present study. The genotype was coded using the additive model. We studied the genetic variant in relation to 2 cardiovascular disease endpoints: (a) MI: fatal or nonfatal MI, and (b) CHD: fatal or nonfatal MI, fatal CHD, sudden death within 1 hour of onset of symptoms, or revascularization (percutaneous coronary artery intervention such as stenting or balloon angioplasty or coronary artery bypass grafting).

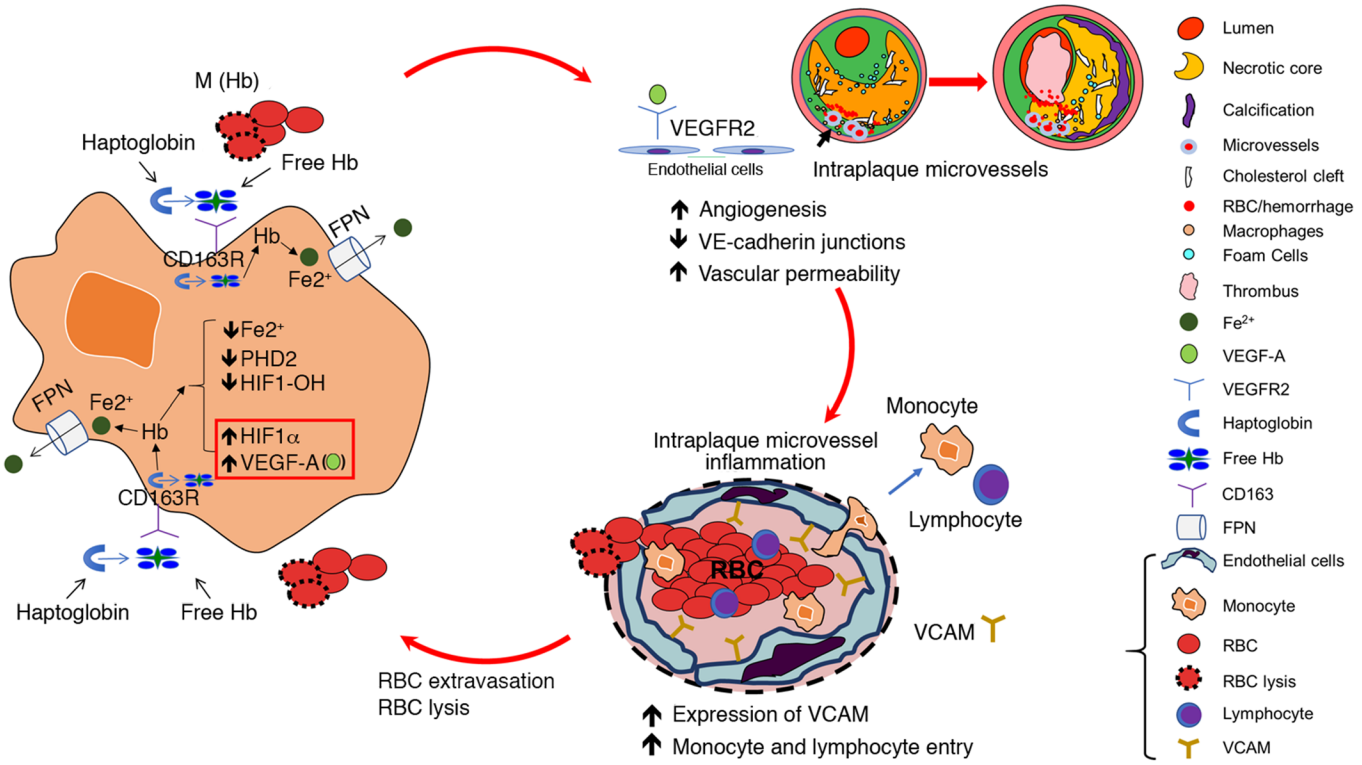

Figure 8. Summary of the role of M(Hb) macrophages in plaque angiogenesis, permeability, vascular inflammation, and plaque progression. In areas of IPH, HH complex ingestion by macrophages induces angiogenesis via activation of HIF1α, which is a consequence of intracellular Fe^{2+} deprivation and PHD2 inhibition. VEGF-A, which is secreted by macrophages via HIF1α activation, promotes angiogenesis, endothelial expression of VCAM, inflammatory cell recruitment, and vascular permeability via VEGF-A/VEGFR2 signaling. This may cause further IPH, RBC lysis, and more Hb ingestion by $CD163^+$ macrophages. This vicious cycle causes plaque progression, which eventually leads to plaque rupture.

Subjects with prevalent CHD at baseline were excluded. The methods by which the incident MI and CHD events were ascertained and classified and the details of quality assurance have been previously published (45). Briefly, participants were contacted annually, and discharge lists from local hospitals and death certificates were surveyed to look for incident MI and CHD events. In total, genotypic and phenotypic data were available for 3,364 ARIC participants of African American ancestry, 3,225 of whom were free of prevalent CHD at baseline and were thus included in the analysis. Cox proportional hazards models were used to examine the association of each genetic variant with incident MI and incident CHD. The seqMeta package (https://cran.r-project.org/web/packages/seqMeta/index.html), implemented in R, was used to perform these analyses. All analyses were adjusted for age, sex, ancestry-informative principal components, and study center. A Bonferroni-corrected significance threshold of 0.025 was used (*P* value 0.05/2 statistical tests).

Study approval. Studies involving the use of deidentified human pathological and autopsy specimens were approved for exempt review by the IRB of the CVPath Institute. Use of the ARIC data was approved by the Committee for the Protection of Human Subjects (CPHS), which serves as the IRB for the University of Texas Health Science Center in Houston. All human participants provided written informed consent to participate in the study. The IACUCs of Emory University and the Medstar Health Research Institute approved all animal protocols. All animal experiments were conducted according to the NIH's *Guide for the Care and Use of Laboratory Animals* (National Academies Press, 2011).

Statistics. Analysis of normality was performed using a Shapiro-Wilk test. Normally and non-normally distributed data were analyzed for significance by Student's *t* test or Mann-Whitney-Wilcoxon tests, respectively. For multiple group comparisons, 1-way ANOVA was applied. If the variance ratio test (F test) was significant, a more detailed post-hoc analysis of differences between groups was made using a Tukey-Kramer honest significant difference test. A *P* value of less than 0.05 was considered statistically significant. See Supplemental Methods for more detailed information.

Author contributions

LG, HA, EH, SLS, FO, RLG, REB, MHD, HJ, RK, HM, QC, FDK, RV, and AVF contributed to the analysis of human atherosclerotic specimens. VK, RP, and HA performed in vitro experiments involving human and mouse macrophages. LG, EH, SLS, REB, CUC, ALJ, and MJL performed mouse experiments and analysis. PSDV, MLG, DEA, EB, ACM, JE, and NS performed SNP analysis. JK, PC, DPC, YZ, and YC provided experimental materials. LG, HA, EH, SLS, PSDV, DEA, HM, MDK, ST, AS, RLG, FDK, DPC, JE, RV, and AVF participated in scientific discussions. LG, HA, AG, MAS, RV, and AVF drafted and/or edited the manuscript, which was critically reviewed by all the authors.

Acknowledgments

This study is supported by the CVPath Institute; the Woodruff Sciences Health Center at Emory University; and the Car-

lyle Fraser Heart Center at Emory Hospital Midtown. CUC is supported by a grant from the CardioVascular Research Foundation (CVRF) of Korea. Genotyping of the CVPath cohort was supported by the National Heart, Lung, and Blood Institute (NHLBI) (HL111089, to NS). The ARIC study was funded in whole or in part with federal funds from the NHLBI, NIH, Department of Health and Human Services (contract numbers HHSN268201700001I, HHSN268201700003I, HHSN268201700005I, HHSN268201700004I, and HHSN268201700021). The authors thank the staff and participants of the ARIC study for their important contributions. Funding support for "Building on GWAS for NHLBI Diseases: the US CHARGE Consortium" was provided by the NIH through the American Recovery and Reinvestment Act of 2009 (ARRA) (5RC2HL102419). The authors thank Daniel McVicar and Marieli Gonzalez-Cotto (National Cancer Institute) and Nicholas Leeper (Stanford University) for helpful discussions and Lila Adams (CVPath Institute) for technical assistance with immunostaining.

Address correspondence to: Aloke V. Finn, CVPath Institute, 19 Firstfield Road, Gaithersburg, Maryland, 20878, University of Maryland School of Medicine, Baltimore, Maryland, 21201, USA. Phone: 301.208.3570; Email: afinn@cvpath.org.

Hirokuni Akahori's present address is: Department of Internal Medicine, Cardiovascular Division, Hyogo College of Medicine, Nishinomiya, Hyogo, Japan.

Emanuel Harari's present address is: Division of Cardiology, Rabin Medical Center, Petah-Tikva, and Sackler Faculty of Medicine, Tel-Aviv University, Tel Aviv, Israel.

Fumiyuki Otsuka's present address is: National Cerebral and Cardiovascular Center, Suita, Osaka, Japan.

Cheol Ung Choi's present address is: Cardiovascular Center, Division of Cardiology, Departments of Internal Medicine, Korea University Guro Hospital, Guro-gu, Seoul, Korea.

1. Ross R. Atherosclerosis--an inflammatory disease. *N Engl J Med*. 1999;340(2):115–126.
2. Guo L, Harari E, Virmani R, Finn AV. Linking Hemorrhage, Angiogenesis, Macrophages, and Iron Metabolism in Atherosclerotic Vascular Diseases. *Arterioscler Thromb Vasc Biol*. 2017;37(4):e33–e39.
3. Moore KJ, Sheedy FJ, Fisher EA. Macrophages in atherosclerosis: a dynamic balance. *Nat Rev Immunol*. 2013;13(10):709–721.
4. Gordon S. Alternative activation of macrophages. *Nat Rev Immunol*. 2003;3(1):23–35.
5. Bouhlel MA, et al. PPARgamma activation primes human monocytes into alternative M2 macrophages with anti-inflammatory properties. *Cell Metab*. 2007;6(2):137–143.
6. Finn AV, et al. Hemoglobin directs macrophage differentiation and prevents foam cell formation in human atherosclerotic plaques. *J Am Coll Cardiol*. 2012;59(2):166–177.
7. Jain RK, Finn AV, Kolodgie FD, Gold HK, Virmani R. Antiangiogenic therapy for normalization of atherosclerotic plaque vasculature: a potential strategy for plaque stabilization. *Nat Clin Pract Cardiovasc Med*. 2007;4(9):491–502.
8. Kolodgie FD, et al. Intraplaque hemorrhage and progression of coronary atheroma. *N Engl J Med*. 2003;349(24):2316–2325.
9. Nagy E, et al. Red cells, hemoglobin, heme, iron, and atherogenesis. *Arterioscler Thromb Vasc Biol*. 2010;30(7):1347–1353.
10. Kristiansen M, et al. Identification of the haemoglobin scavenger receptor. *Nature*. 2001;409(6817):198–201.
11. Pulford K, Micklem K, McCarthy S, Cordell J, Jones M, Mason DY. A monocyte/macrophage antigen recognized by the four antibodies GHI/61, Ber-MAC3, Ki-M8 and SM4. *Immunology*. 1992;75(4):588–595.
12. Boyle JJ, et al. Activating transcription factor 1 directs Mhem atheroprotective macrophages through coordinated iron handling and foam cell protection. *Circ Res*. 2012;110(1):20–33.
13. Boyle JJ, et al. Coronary intraplaque hemorrhage evokes a novel atheroprotective macrophage phenotype. *Am J Pathol*. 2009;174(3):1097–1108.
14. Habib A, et al. Hepcidin-ferroportin axis controls toll-like receptor 4 dependent macrophage inflammatory responses in human atherosclerotic plaques. *Atherosclerosis*. 2015;241(2):692–700.
15. Ivan M, et al. HIFalpha targeted for VHL-mediated destruction by proline hydroxylation: implications for O2 sensing. *Science*. 2001;292(5516):464–468.
16. Nandal A, et al. Activation of the HIF prolyl hydroxylase by the iron chaperones PCBP1 and PCBP2. *Cell Metab*. 2011;14(5):647–657.
17. Berra E, Benizri E, Ginouvès A, Volmat V, Roux D, Pouysségur J. HIF prolyl-hydroxylase 2 is the key oxygen sensor setting low steady-state levels of HIF-1alpha in normoxia. *EMBO J*. 2003;22(16):4082–4090.
18. Otsuka F, et al. Community-based statins and advanced carotid plaque: Role of CD163 positive macrophages in lipoprotein-associated phospholipase A2 activity in atherosclerotic plaque. *Atherosclerosis*. 2017;267:78–89.
19. Sluimer JC, et al. Thin-walled microvessels in human coronary atherosclerotic plaques show incomplete endothelial junctions relevance of compromised structural integrity for intraplaque microvascular leakage. *J Am Coll Cardiol*. 2009;53(17):1517–1527.
20. Bobryshev YV, Cherian SM, Inder SJ, Lord RS. Neovascular expression of VE-cadherin in human atherosclerotic arteries and its relation to intimal inflammation. *Cardiovasc Res*. 1999;43(4):1003–1017.
21. Boneu B, Abbal M, Plante J, Bierme R. Letter: Factor-VIII complex and endothelial damage. *Lancet*. 1975;1(7922):1430.
22. Bories G, et al. Liver X receptor activation stimulates iron export in human alternative macrophages. *Circ Res*. 2013;113(11):1196–1205.
23. Nemeth E, et al. Hepcidin regulates cellular iron efflux by binding to ferroportin and inducing its internalization. *Science*. 2004;306(5704):2090–2093.
24. Bates DO. Vascular endothelial growth factors and vascular permeability. *Cardiovasc Res*. 2010;87(2):262–271.
25. Akahori H, et al. CD163 interacts with TWEAK to regulate tissue regeneration after ischaemic injury. *Nat Commun*. 2015;6:7792.
26. Sindrilaru A, et al. An unrestrained proinflammatory M1 macrophage population induced by iron impairs wound healing in humans and mice. *J Clin Invest*. 2011;121(3):985–997.
27. Etzerodt A, Kjolby M, Nielsen MJ, Maniecki M, Svendsen P, Moestrup SK. Plasma clearance of hemoglobin and haptoglobin in mice and effect of CD163 gene targeting disruption. *Antioxid Redox Signal*. 2013;18(17):2254–2263.
28. Rosenfeld ME, Polinsky P, Virmani R, Kauser K, Rubanyi G, Schwartz SM. Advanced atherosclerotic lesions in the innominate artery of the ApoE knockout mouse. *Arterioscler Thromb Vasc Biol*. 2000;20(12):2587–2592.
29. Cybulsky MI, et al. A major role for VCAM-1, but not ICAM-1, in early atherosclerosis. *J Clin Invest*. 2001;107(10):1255–1262.
30. O'Brien KD, McDonald TO, Chait A, Allen MD, Alpers CE. Neovascular expression of E-selectin, intercellular adhesion molecule-1, and vascular cell adhesion molecule-1 in human atherosclerosis and their relation to intimal leukocyte content. *Circulation*. 1996;93(4):672–682.
31. Kim I, Moon SO, Kim SH, Kim HJ, Koh YS, Koh GY. Vascular endothelial growth factor expression of intercellular adhesion molecule 1 (ICAM-1), vascular cell adhesion molecule 1 (VCAM-1), and E-selectin through nuclear factor-kappa B activation in endothelial cells. *J Biol Chem*. 2001;276(10):7614–7620.
32. Kamatani Y, et al. Genome-wide association study of hematological and biochemical traits in a Japanese population. *Nat Genet*. 2010;42(3):210–215.
33. Wartman WB. Occlusion of the coronary arter-

ies by hemorrhage into their walls. *Am Heart J*. 1938;15:459–470.
34. Barger AC, Beeuwkes R, Lainey LL, Silverman KJ. Hypothesis: vasa vasorum and neovascularization of human coronary arteries. A possible role in the pathophysiology of atherosclerosis. *N Engl J Med*. 1984;310(3):175–177.
35. Sluimer JC, et al. Hypoxia, hypoxia-inducible transcription factor, and macrophages in human atherosclerotic plaques are correlated with intraplaque angiogenesis. *J Am Coll Cardiol*. 2008;51(13):1258–1265.
36. Marsch E, et al. Deficiency of the oxygen sensor prolyl hydroxylase 1 attenuates hypercholesterolaemia, atherosclerosis, and hyperglycaemia. *Eur Heart J*. 2016;37(39):2993–2997.
37. Sun J, Underhill HR, Hippe DS, Xue Y, Yuan C, Hatsukami TS. Sustained acceleration in carotid atherosclerotic plaque progression with intraplaque hemorrhage: a long-term time course study. *JACC Cardiovasc Imaging*. 2012;5(8):798–804.
38. Nazer B, Humphreys BD, Moslehi J. Effects of novel angiogenesis inhibitors for the treatment of cancer on the cardiovascular system: focus on hypertension. *Circulation*. 2011;124(15):1687–1691.
39. Nikpay M, et al. A comprehensive 1,000 Genomes-based genome-wide association meta-analysis of coronary artery disease. *Nat Genet*. 2015;47(10):1121–1130.
40. Virmani R, Kolodgie FD, Burke AP, Farb A, Schwartz SM. Lessons from sudden coronary death: a comprehensive morphological classification scheme for atherosclerotic lesions. *Arterioscler Thromb Vasc Biol*. 2000;20(5):1262–1275.
41. Golubeva YG, Smith RM, Sternberg LR. Optimizing Frozen Sample Preparation for Laser Microdissection: Assessment of CryoJane Tape-Transfer System®. *PLoS One*. 2013;8(6):e66854.
42. The Atherosclerosis Risk in Communities (ARIC) Study: design objectives. The ARIC investigators. *Am J Epidemiol*. 1989;129(4):687–702.
43. Grove ML, et al. Best practices and joint calling of the HumanExome BeadChip: the CHARGE Consortium. *PLoS ONE*. 2013;8(7):e68095.
44. Psaty BM, et al. Cohorts for Heart and Aging Research in Genomic Epidemiology (CHARGE) Consortium: Design of prospective meta-analyses of genome-wide association studies from 5 cohorts. *Circ Cardiovasc Genet*. 2009;2(1):73–80.
45. White AD, et al. Community surveillance of coronary heart disease in the Atherosclerosis Risk in Communities (ARIC) Study: methods and initial two years' experience. *J Clin Epidemiol*. 1996;49(2):223–233.